Hypoxia causes pancreatic β-cell dysfunction by activating a transcriptional repressor BHLHE40

Tomonori Tsuyama[1], Yoshifumi Sato[2,*], Tatsuya Yoshizawa[2], Takaaki Matsuoka[3], Kazuya Yamagata[1,2,*]

[1]Center for Metabolic Regulation of Healthy Aging (CMHA), Faculty of Life Sciences, Kumamoto University, Kumamoto 860-8556, Japan.

[2]Department of Medical Biochemistry, Faculty of Life Sciences, Kumamoto University, Kumamoto 860-8556, Japan.

[3]First Department of Internal Medicine, Wakayama Medical University, Wakayama 641-8509, Japan.

*Corresponding author: Kazuya Yamagata, Department of Medical Biochemistry, Faculty of Life Sciences, Kumamoto University, 1-1-1 Honjo, Kumamoto 860-8556, Japan. Phone: +81-96-373-5068; Email: k-yamaga@kumamoto-u.ac.jp.

*Corresponding author: Yoshifumi Sato, Department of Medical Biochemistry, Faculty of Life Sciences, Kumamoto University, 1-1-1 Honjo, Kumamoto 860-8556, Japan. Phone: +81-96-373-5070; Email: ysato413@kumamoto-u.ac.jp.

Conflict-of-interest

The authors have declared that no conflict of interest exists.

ABSTRUCT

Hypoxia can occur in pancreatic β-cells in type 2 diabetes. Although hypoxia exerts deleterious effects on β-cell function, the associated mechanisms are largely unknown. Here, we show that the transcriptional repressor basic helix-loop-helix family member e40 (BHLHE40) is highly induced in hypoxic mouse and human β-cells and suppresses insulin secretion. Conversely, BHLHE40 deficiency in hypoxic MIN6 cells or in the β-cells of *ob/ob* mice reversed the insulin secretion. Mechanistically, BHLHE40 represses expression of *Mafa*, which encodes the transcription factor musculoaponeurotic fibrosarcoma oncogene family A (MAFA), by attenuating binding of pancreas/duodenum homeobox protein 1 (PDX1) to its enhancer region. Impaired insulin secretion in hypoxic β-cells was recovered by MAFA expression. Collectively, this work identifies BHLHE40 as a key hypoxia-induced transcriptional repressor in β-cells and its implication in the β-cell dysfunction in type 2 diabetes.

INTRODUCTION

Glucose metabolism is regulated by crosstalk between pancreatic β-cells and insulin-sensitive tissues. In case of insulin resistance, β-cells increase insulin secretion to maintain normal glucose tolerance. However, when β-cells are incapable of this task, plasma concentrations of glucose increase. Prolonged exposure to hyperglycaemia has deleterious effects on β-cell function through various mechanisms, including oxidative stress, endoplasmic reticulum (ER) stress, and inflammation and contributes to the development and progression of type 2 diabetes (1-3). Because β-cells are highly dependent on oxidative phosphorylation for adenosine triphosphate (ATP) production and insulin secretion, high glucose conditions generate intracellular hypoxia due to large amounts of oxygen consumption. Importantly, hypoxia was shown to occur *in vivo* in islets in animal models of type 2 diabetes (4-7). Like oxidative and ER stress, hypoxia leads to β-cell dysfunction and loss of β-cells, supporting the idea that hypoxia is another mechanism leading to β-cell failure in type 2 diabetes (8-11).

Hypoxia-inducible factor (HIF), a heterodimeric transcription factor consisting of an oxygen-sensitive HIF-α subunit and a constitutively expressed HIF-1β subunit, plays critical roles in the cellular responses to hypoxia (12, 13). HIF induces the expression of a number of genes necessary for adaptation to hypoxia, including those

involved in glycolysis, erythropoiesis, and angiogenesis. However, hyperactivation of HIF in β-cells impairs insulin secretion by switching glucose metabolism from aerobic oxidative phosphorylation to anaerobic glycolysis (14-16), suggesting that activation of HIF underlies β-cell dysfunction and glucose intolerance in hypoxia. Besides gene induction, transcriptional repression of genes also occurs in response to hypoxia and was found to involve several transcription repressors, such as RE1 silencing transcription factor (REST), BTB and CNC homology 1 (BACH1), zinc finger E- box binding homeobox 1 (ZEB1), and inhibitor of DNA binding 2 (ID2) (17). Previously, we reported that hypoxia causes the downregulation of a number of β-cell genes involved in insulin secretion in mouse islets and MIN6 β-cells (9). However, the mechanisms of hypoxia-induced transcriptional repression in β-cells and the contribution of gene repression to β-cell dysfunction are largely unknown.

In the present study, we identified the transcriptional repressor basic helix-loop-helix family member e40 (BHLHE40) as being highly induced in β-cells under hypoxic conditions and found that it inhibits glucose-stimulated insulin secretion by suppressing transcription of *Mafa*, which encodes musculoaponeurotic fibrosarcoma oncogene family A (MAFA), a transcription factor that plays critical roles in insulin secretion. We also showed that BHLHE40 deficiency reversed decreased insulin secretion by hypoxic β-

cells *in vitro* and *in vivo*. Our findings present a new scenario in which hypoxia impairs β-cell function through activation of the transcriptional repressor BHLHE40.

RESULTS

Global gene expression in hypoxic β-cells and islets

To assess the impact of hypoxia on global gene expression of β-cells, we first performed RNA sequencing (RNA-seq) on both mouse and human islets cultured under normal and low oxygen conditions. Approximately 5% of expressed mRNAs were significantly downregulated at least 1.5-fold in hypoxic compared with non-hypoxic islets (mouse, 20% vs 5%, respectively; human, 20% vs 2%, respectively; Supplemental Figure 1A). Consistent with our previous findings (9), under hypoxic conditions the expression of a number of β-cell genes with important roles in insulin secretion was decreased in islets (Figure 1A). Gene set enrichment analysis (GSEA) revealed that two hallmark gene sets (pancreas beta cells and oxidative phosphorylation) were significantly downregulated in both mouse and human islets in hypoxia and one hallmark gene set (hypoxia) was significantly upregulated (Figure 1B and Supplemental Figure 1B). We hypothesized that transcriptional repressors are involved in the suppression of β-cell genes under hypoxic conditions. To identify the hypoxia-sensitive repressors in β-cells, we compared the RNA-

seq–based data of hypoxia-induced genes in mouse islets, human islets, and MIN6 cells and found that 25 genes were elevated (Figure 1C). By analyzing the gene ontology of these genes, we discovered that activating transcription factor 3 (ATF3) and BHLHE40 are associated with transcriptional repression (Figure 1C). In addition, BHLHE41, REST, BACH1, ID1, ID2, ZEB1/ZEB2, and SNAI1 were reported elsewhere to function as hypoxia-induced transcriptional repressors (17). Among all these repressor genes, in our study, *Bhlhe40* mRNA was the most significantly increased in hypoxic mouse islets, human islets, and MIN6 cells (Figures 1, D-F). BHLHE40 (also referred to as DEC1/SHARP2/STRA13) is a member of the basic helix-loop-helix (bHLH) family and functions primarily as a transcriptional repressor by binding to DNA at class B E-box motifs (18). It plays pivotal roles in many biological processes, including cellular differentiation, cell growth, growth arrest, circadian rhythm, immunological response, and hypoxia, but its biological function in β-cells is unknown. Accordingly, we focused on the role of BHLHE40 in hypoxic β-cells.

Regulation of *Bhlhe40* expression in hypoxic β-cells and islets

BHLHE40 was expressed ubiquitously in adult mouse tissues, including pancreatic islets and MIN6 cells (Figure 2A and Supplemental Figure 2A). Hypoxia

rapidly increased the expression of *Bhlhe40* mRNA, i.e., within 3 hours, but a marked upregulation of BHLHE40 protein was noted at 12 hours and this upregulation persisted at 24 hours in MIN6 cells (Figure 2B and Supplemental Figure 2B). Increased BHLHE40 expression in hypoxia was also detected in mouse islets (Figure 2C and Supplemental Figure 2C).

Hypoxia induces oxidative and ER stress and activation of AMP-activated protein kinase (AMPK) (6, 19, 20). However, in our study, oxidative stress (caused by treatment with H_2O_2), ER stress (caused by treatment with thapsigargin or tunicamycin), and AMPK activation (caused by treatment with metformin) did not increase expression of *Bhlhe40* mRNA in MIN6 cells (Figures 2, D-F), suggesting that these processes are not involved in the induction of *Bhlhe40*. Previous studies showed that HIF-1 is involved in hypoxia-induced *Bhlhe40* expression (21, 22). Consistent with this finding, hypoxia-induced *Bhlhe40* mRNA expression was partially inhibited by suppression of HIF-1β (Figure 2G and Supplemental Figure 2D), indicating that hypoxia-induced *Bhlhe40* expression is partially HIF dependent in β-cells. We and others demonstrated that hypoxia occurs in islets in animal models of type 2 diabetes (4-6). Consistent with this finding, levels of *Bhlhe40* mRNA and BHLHE40 were significantly elevated (2.3-fold and 4.5-fold, respectively) in islets of *ob/ob* mice (Figures 2, H and I). Upregulation of BHLHE40

was detected also in islets of *db/db* mice (Figure 2J and Supplemental Figure 2E). Intracellular localization of BHLHE40 varies by cells (23). Immunohistochemical analysis revealed strong BHLHE40 immunoreactivity in the cytoplasm of islets in *ob*/*ob* mice, but BHLHE40 staining was clearly detected also in the nucleus of islets (Figure 2K). The nuclear localization of BHLHE40 supports its function as a transcriptional repressor.

BHLHE40 controls insulin secretion in β-cells

To explore the role of BHLHE40 in β-cells, we generated *Bhlhe40* knockdown (KD) MIN6 cells (Supplemental Figure 3A). Although BHLHE40 is reported to be involved in cell cycle and apoptosis regulation (24), hypoxia-induced growth inhibition (Supplemental Figure 3B) and cell death (Supplemental Figure 3C) were not restored in *Bhlhe40* KD MIN6 cells. Next, we investigated the impact of *Bhlhe40* KD on glucose-stimulated insulin secretion. As described previously (9), insulin secretion by high glucose was significantly decreased under hypoxic conditions without affecting insulin content (Figures 3, A and B). Of note, *Bhlhe40* KD significantly restored hypoxia-related decreased insulin secretion (Figure 3A), and conversely, BHLHE40 overexpression significantly attenuated insulin secretion (Figure 3C and Supplemental Figure 3D). These

163 results indicate that BHLHE40 is involved in suppressing the glucose-stimulated insulin
164 secretion. Glucose-stimulated insulin secretion occurs after the generation of ATP through
165 the metabolism of glucose. The increase of the ATP/ADP ratio leads to closure of ATP-
166 sensitive K^+ channels, membrane depolarization, an increase of cytosolic $[Ca^{2+}]_i$ via
167 activation of voltage-dependent Ca^{2+} channels, and eventually the exocytosis of insulin-
168 containing secretory granules (25).

169 High K^+ induced membrane depolarization evokes Ca^{2+} dependent insulin
170 exocytosis from β-cells. We next investigated the role of BHLHE40 on KCl-stimulated
171 insulin secretion. As in the case of glucose, a significant decrease in KCl-stimulated
172 insulin secretion was detected in hypoxic MIN6 cells but not in hypoxic *Bhlhe40* KD
173 MIN6 cells (Figure 3D). KCl produced a significantly smaller insulin secretion in MIN6
174 cells overexpressing BHLHE40 than in control MIN6 cells (Figure 3E). The observation
175 that KCl induced an equivalent increase of $[Ca^{2+}]_i$ levels in both cells overexpressing
176 BHLHE40 and control cells (Figures 3, F and G) suggests that BHLHE40 affects steps
177 after $[Ca^{2+}]_i$ elevation. Next, we further explored the role of BHLHE40 on exocytosis by
178 transfecting MIN6 cells with a human growth factor (hGH) expression vector. In
179 transfected cells, hGH is targeted to insulin-containing secretory granules, and hGH
180 release can be used to monitor exocytosis from the cells (26, 27). As shown in Figure 3H,

KCl-induced hGH secretion was significantly decreased under hypoxic conditions, and the decrease was almost completely reversed by *Bhlhe40* KD. These results emphasize the role of BHLHE40 in exocytosis in MIN6 cells.

To investigate the possibility that BHLHE40 affects multiple steps during glucose-stimulated insulin secretion, we next examined glucose uptake in *Bhlhe40* KD and control MIN6 cells. Uptake of 2-NBDG, a fluorescent derivative of glucose, was decreased by hypoxia, but *Bhlhe40* KD did not affect 2-NBDG uptake in MIN6 cells (Figure 3I), indicating that BHLHE40 does not affect glucose uptake. In line with our previous study (9), ATP levels in MIN6 cells were decreased under hypoxic conditions, and the decrease of ATP levels was significantly restored by *Bhlhe40* KD (Figure 3J). In agreement with these results, under hypoxic conditions, the decreased mitochondrial mass was significantly increased by *Bhlhe40* KD in MIN6 cells (Figure 3K). Taken together, our results show that BHLHE40 affects at least two different steps, i.e., ATP generation and exocytosis, during insulin secretion.

BHLHE40 suppresses *Mafa* expression in β-cells

To further understand how BHLHE40 regulates insulin secretion, we performed RNA-seq analysis in control MIN6 cells and MIN6 cells overexpressing *Bhlhe40*.

Compared with control MIN6 cells, MIN6 cells overexpressing *Bhlhe40* showed 2630 differentially expressed genes (1288 downregulated and 1342 upregulated; adjusted $p < 0.01$) (Figure 4A). Gene ontology analysis revealed that the downregulated genes included transcription genes with critical roles during insulin secretion, including *Mafa*, *Nkx2-2*, *Ppargc1a, Vdr*, *Nkx6-1*, and *Neurod1* (Figures 4, A and B). Quantitative real-time polymerase chain reaction (qRT-PCR) in independent samples confirmed the significant downregulation of *Mafa*, *Nkx2-2*, *Ppargc1a*, and *Vdr* expression by *Bhlhe40* overexpression (Figure 4C). To validate that BHLHE40 functions as a repressor of these genes, we next examined their expression in *Bhlhe40* KD MIN6 cells under hypoxic conditions. Hypoxia significantly decreased *Mafa*, *Ppargc1a, Vdr,* and *Nkx6-1* mRNA, but downregulation of *Mafa* was completely restored by KD of BHLHE40 (Figure 4D). At the protein level, suppression of MAFA by BHLHE40 and restoration of hypoxia-induced downregulation of MAFA by BHLHE40 deficiency were also detected (Figures 4, E and F). MAFA regulates genes required for insulin exocytosis, including *Stxbp1* (encoding MUNC18-1), *Napa* (encoding N-ethylmaleimide-sensitive factor attachment protein), *Syt7* (encoding synaptotagmin 7), and *Stx1a* (encoding syntaxin1A) (28-33). Under hypoxic conditions, *Bhlhe40* KD also significantly restored the downregulation of *Stxbp1*, *Napa*, *Syt7*, and *Stx1a* (Figure 4G). MAFA plays a critical role in both glucose-

and KCl-stimulated insulin secretion (28, 34). Intriguingly, the glucose- and KCl-related decreased insulin secretion in hypoxic conditions was significantly restored by adeno-associated virus (AAV)-mediated overexpression of *Mafa* (Figures 4, H and I, and Supplemental Figure 4). These results indicate that BHLHE40 suppresses insulin secretion, at least in part, by reducing the expression of MAFA in β-cells.

Peroxisome proliferator-activated receptor-γ coactivator 1-α (PGC-1α), which is encoded by *Ppargc1a*, regulates mitochondrial biogenesis and oxidative phosphorylation (35). Previous studies revealed that BHLHE40 acts as a transcriptional repressor of *Ppargc1a* (36, 37). Consistent with this finding, *Ppargc1a* expression was significantly downregulated by *Bhlhe40* overexpression in MIN6 cells, and the hypoxia-induced downregulation of *Ppargc1a* was recovered by KD of *Bhlhe40* (Figures 4, C and D), indicating that *Ppargc1a* is another target gene of BHLHE40 in MIN6 cells. In these experimental conditions, BHLHE40 KD did not affect the expression of *Nkx2-2*, *Vdr,* *Nkx6-1,* or *Neurod1* mRNAs (Figure 4D).

BHLHE40 controls *Mafa* expression *via* two E-box sites in the enhancer region

To further explore the mechanism by which BHLHE40 suppresses *Mafa* expression in β-cells, we performed a reporter gene assay with a reporter plasmid. We

235 included the mouse *Mafa* enhancer/promoter region (-10427 to +22 bp to transcriptional
236 start site) because it shows maximum *Mafa* promoter activity in β-cells (38, 39). *Mafa*
237 reporter gene activity was significantly decreased under hypoxic conditions, but the
238 reduction was abolished by *Bhlhe40* KD (Figure 5A). BHLHE40 binds to E-box sequence
239 (5'-CANNTG-3') to suppress its target genes. Screening of the JASPAR database (40)
240 revealed four E-box sites (A, -9909/-9899; B, -8705/-8695; C, -6987/-6976; and D, -
241 4949/4938, relative score > 0.9) within the -10427/+22 region (Figure 5B).
242 Overexpression of *Bhlhe40* suppressed activity of the reporter gene in MIN6 cells, but
243 mutation of the A or C site in the reporter gene abolished the reduction of transcriptional
244 activity by BHLHE40 (Figure 5C). Consistent with this finding, suppression of the
245 reporter gene activity by hypoxia also was attenuated by mutation of these two sites
246 (Figure 5D). Furthermore, chromatin immunoprecipitation (ChIP) assay revealed
247 enhanced binding of BHLHE40 to A and C sites in MIN6 cells under hypoxic conditions
248 (Figure 5E). These results indicate that BHLHE40 suppresses *Mafa* expression by binding
249 to the A or C site. BHLHE40 is reported to repress transcription of the target genes by
250 recruiting histone deacetylase (HDAC; ref. 41, 42). However, treatment with trichostatin
251 A (TSA), an HDAC inhibitor, failed to affect the reduced reporter gene activity in hypoxic
252 MIN6 cells (Figure 5F).

253 The transcription factor pancreas/duodenum homeobox protein 1 (PDX1) was
254 reported to regulate *Mafa* expression in β-cells by binding to the enhancer region (-8152
255 to -7780 relative to the transcription start site) (38, 43). Therefore, we investigated
256 whether BHLHE40 represses *Mafa* expression by inhibiting PDX1 binding. Intriguingly,
257 the ChIP assay revealed that BHLHE40 significantly reduced PDX1 binding to the *Mafa*
258 gene in MIN6 cells (Figure 5G). These results suggest that BHLHE40 controls *Mafa*
259 expression, at least in part, by affecting the binding of PDX1.
260
261 **Deficiency of BHLHE40 improves hyperglycaemia in *ob/ob* mice**
262 To evaluate the role of BHLHE40 *in vivo*, we generated β-cell–specific
263 BHLHE40 knockout (*βB40*KO) mice by crossing Pdx1-Cre mice (44) with floxed
264 *Bhlhe40* (*Bhlhe40*^{fl}) mice (Supplemental Figures 5, A and B). Body weight (Supplemental
265 Figure 5C) and nonfasting blood glucose concentration (Supplemental Figure 5D) were
266 similar in *βB40*KO and *Bhlhe40*$^{fl/fl}$ mice, and the intraperitoneal glucose tolerance test
267 also showed no differences in blood glucose levels among Pdx1-Cre, *Bhlhe40*$^{fl/fl}$, and
268 *βB40*KO mice (Figure 6A).
269 BHLHE40 negatively regulates insulin secretion, and BHLHE40 expression was
270 markedly upregulated in *ob/ob* pancreatic islets (Figure 2I). We then investigated the

271 effects of β-cell–specific BHLHE40 deficiency in *ob/ob* mice (*βB40*KO:*ob/ob* mice). In
272 these mice, BHLHE40 deficiency in β-cells had no effect on obesity (Figure 6B) or insulin
273 sensitivity (Supplemental Figure 5E). However, the mice displayed better glucose
274 tolerance than control *Bhlhe40*$^{fl/fl}$:*ob*/*ob* (control:*ob*/*ob*) mice (Figures 6, C and D). In
275 agreement with the results obtained in MIN6 cells, glucose-stimulated insulin secretion
276 was significantly increased in *βB40*KO:*ob/ob* mice (Figure 6E). Insulin secretion by high
277 glucose (Figure 6F) and KCl (Figure 6G) was also increased in *βB40*KO islets under
278 hypoxic conditions. We measured the ATP content with 2.2mM and 22mM glucose under
279 hypoxic conditions and found that ATP levels were significantly increased in *βB40*KO
280 islets compared with control islets (Figure 6H). There was no significant difference in the
281 ratio of β-cell area to whole pancreas area between *βB40*KO:*ob/ob* and control:*ob*/*ob*
282 mice (Figures 6, I and J), but stronger nuclear immunostaining of MAFA was detected in
283 *βB40*KO:*ob/ob* mice (Figures 6, K and L). Lastly, the increased expression of *Mafa,*
284 *Stxbp1*, *Napa*, *Syt7*, *Stx1a*, and *Ppargc1a* in *βB40*KO:*ob/ob* islets was confirmed by qRT-
285 PCR (Figure 6M). Taken together, the results show that BHLHE40 deficiency improves
286 glucose tolerance in *ob/ob* mice by enhancing insulin secretion.
287
288

DISCUSSION

Adaptation to hypoxia involves 3 major responses: increased glycolysis to cope with ATP depletion, increased oxygen delivery, and inhibition of energy-demanding processes such as gene transcription (17). HIF transcriptional factors are known to play central roles in glycolytic ATP production and oxygen delivery, but the mechanisms underlying transcriptional repression in hypoxia are poorly understood. By screening hypoxia-induced genes in mouse and human islets and MIN6 cells, we showed that the transcriptional repressor BHLHE40 is highly induced in hypoxic β-cells. We also demonstrated that BHLHE40 negatively regulates insulin secretion by suppressing transcription of *Mafa*. Hypoxia is involved in β-cell dysfunction, and the contribution of HIF-1 to this process is well established (7, 14-16). However, our present findings present a novel scenario in which hypoxia decreases insulin secretion by inducing BHLHE40 (Figure 7).

BHLHE40 was previously reported to suppress transcription of target genes by recruiting HDACs (37, 45). In contrast, we found that TSA treatment did not relieve the BHLHE40-mediated repression of *Mafa*, indicating that *Mafa* repression by BHLHE40 is independent of the recruitment of HDAC. On the other hand, we demonstrated that BHLHE40 inhibits the binding of PDX1 to the critical enhancer region of *Mafa*.

Repressors are reported to regulate transcription by interacting with activator proteins (46). BHLHE40 might suppress *Mafa* transcription by interacting with PDX1. Alternatively, BHLHE40 might change DNA conformations by recruiting chromatin-remodeling factors. The family of large Maf proteins comprises MAFA, MAFB, and MAF (c-Maf). Intriguingly, recent studies demonstrated that BHLHE40 represses the expression of *Mafb* and *Maf* mRNAs in macrophages (47). Thus, BHLHE40 seems to be a common repressor of the large-Maf family. Further studies are necessary to clarify the mechanism by which BHLHE40 suppresses these genes. Moreover, we also revealed that BHLHE40 suppresses transcription of *Ppargc1a* and decreases ATP levels in β-cells. Because PGC-1α plays important roles in ATP production (48, 49), it is plausible that the decreased expression of PGC-1α may be involved in the reduced ATP levels and impaired insulin secretion under hypoxic conditions.

In the present study, we showed that approximately 5% of genes were downregulated in hypoxic islets. In addition to BHLHE40, we also found an increased expression of ATF3 in β-cells in hypoxia. Previously, ATF3 was reported to function as a transcriptional repressor and to suppress genes related to glucose metabolism, such as *Irs2*, *Nrf1*, and *Pparg* (50, 51). Thus, hypoxia might affect β-cell function through not only BHLHE40 but also other transcriptional repressors, such as ATF3.

In conclusion, we identified BHLHE40 as a novel hypoxia-induced transcriptional repressor that negatively regulates insulin secretion in β-cells. Because β-cell dysfunction in type 2 diabetes is progressive, new approaches to slow the progression are needed. Inhibition of BHLHE40 might be a new therapeutic strategy for preventing the β-cell dysfunction by hypoxia.

METHODS

Mouse models. C57B6 wild-type (WT), *ob/ob*, and *db/db* mice were purchased from KBT Oriental Co., Ltd. (Saga, Japan). Mice carrying the Bhlhe40$^{tm1a(KOMP)Wtsi}$ allele (C57BL/6NTac-Bhlhe40tm1a(KOMP)Wtsi/WtsiPh, EM:09819) were obtained from the European Conditional Mouse Mutagenesis Program (EUCOMM) and crossed with *FLPe* mice (B6-Tg(CAG-FLPe)36, RBRC01834, RIKEN BRC, Ibaraki, Japan) to remove a LacZ reporter and a Neo cassette flanked by two Frt sites. To achieve a *Bhlhe40* deletion in β-cells, Bhlhe40$^{fl/fl}$ mice were further crossed with Pdx1-Cre mice (gift from Dr. Douglas A. Melton). β-cell–specific Bhlhe40 knockout mice on *ob/ob* background were generated by crossing with Bhlhe40$^{fl/fl}$:*ob*/+ mice and Pdx1-Cre:Bhlhe40$^{fl/fl}$:*ob*/+ mice. Mice were housed under a 12-hour light/dark cycle with free access to water and normal chow (CE-2; CLEA, Tokyo, Japan). Room temperature was maintained at 22 ± 1-2°C.

Human pancreatic islets. Human islets were commercially purchased from Prodo Laboratories (Irvine, CA). The cadaveric donor had no history of diabetes (32-year-old male; BMI, 25.1; HbA1c, 5.1%). Islets were cultured according to the Prodo Laboratories instructions.

Cell lines. MIN6 cells were gifts from Jun-ichi Miyazaki (Osaka University). They were maintained in Dulbecco's modified Eagle's medium (DMEM) supplemented with 10% (v/v) fetal bovine serum (FBS), 0.1% (v/v) penicillin/streptomycin (P/S), and 50μM β-mercaptoethanol at 37°C in 5% CO_2, 95% air. For the hypoxic cell culture, a multi-gas incubator (APM-300; ASTEC, Fukuoka, Japan) was used. Retroviral packaging cell line Platinum-E (Plat-E; RV-101) cells were purchased from Cell Biolabs, Inc. (San Diego, CA). They were maintained in DMEM supplemented with 10% (v/v) FBS and 0.1% (v/v) P/S at 37°C in 5% CO_2, 95% air. 293AAV cells were purchased from Cell Biolabs Inc. (AAV-100). They were maintained in DMEM with sodium pyruvate supplemented with 10% (v/v) FBS, 1x Glutamax, 1x Opti-MEM, and 0.1% (v/v) P/S at 37°C in 5% CO_2, 95% air.

Plasmids. The HA-tagged mouse *Bhlhe40* coding sequence was excised from a pCAGGS-DEC1 plasmid (RDB08473, Riken, Saitama, Japan; ref. 52) and subcloned into pcDNA3.1 and pMXs-Puro Retroviral vector (RTV-012, Cell Biolabs, Inc.). For knockdown experiments, oligonucleotide encoding Bhlhe40 short hairpin RNA (shRNA; target sequence: 5'-GCACGTGAAAGCATTGACA-3'; ref. 53) and Hif1β shRNA (target sequence: 5'-GGACAGAGATCCAAGGTTT-3') were cloned into the pSIREN-RetroQ expression vector (631526; Clontech Laboratories Inc., Mountain View, CA). The FLAG-tagged mouse *Pdx1* coding sequence was amplified by PCR and subcloned into a pMXs-Neo Retroviral vector (RTV-011, Cell Biolabs, Inc.). pGL3-basic-MafA plasmid (-10427/+22 from transcription start site) was previously reported (39). The pGL3-basic-MafA plasmids with single deletion of the E-box site at -9910/-9899 (A; GAAAAATGCTG), -8706/-8695 (B; TGAAAATGATT), or -6987/-6976 (C; GGAAAATGCCT) were generated with a KOD-Plus Mutagenesis Kit (SMK-101, TOYOBO, Osaka, Japan). The truncated pGL3-basic-MafA plasmid (-5811/+22) was generated by BglII digestion and re-ligation. The mouse *Mafa* coding sequence was amplified by PCR and subcloned into pAAV-MCS (VPK-410, Cell Biolabs. Inc.).

MIN6 cells stably overexpressing/silencing a target gene. To generate stable

overexpression cell lines, retroviral vectors (pMx-Puro-HA-*Bhlhe40*, pMx-Puro Control, pMx-Neo FLAG-*Pdx1* or pMx-Neo Control plasmid) were transfected into Plat-E cells with JetPRIME transfection reagent (114-15, Polyplus, New York, NY), and MIN6 cells were infected with the respective retroviruses and selected by incubation with puromycin (5 μg/ml) for 2 days or G418 (500 μg/ml) for 4 weeks. For stable knockdown of *Bhlhe40*, pSIREN-RetroQ-Bhlhe40 or pSIREN-RetroQ-control vector was transfected into Plat-E cells, and MIN6 cells were infected with the retroviruses and selected by incubation with puromycin (5 μg/ml) for 2 days.

AAV-*Mafa* preparation. 293AAV cells were plated onto 10-cm dishes. At 80% confluency, cells were transfected with 2 μg/dish pAAV-DJ, 3 μg/dish pHelper, and either 2 μg/dish pAAV-GFP or pAAV-*Mafa* with JetPRIME transfection reagent. Three days after transfection, AAV-GFP and AAV-*Mafa* were purified with the AAV pro Extraction Solution Kit (6235, Takara, Shiga, Japan), and the titers were determined with a Quick Titer AAV Quantification Kit (VPK-145, Cell Biolabs, Inc.) according to the manufacturer's instructions.

Isolation of mouse islets. Mice were euthanized by cervical dislocation and subjected to

bile duct cannulation and digestion of the pancreas with a mixture of collagenase P (11-249-002-001, Roche, Basel, Switzerland), hyaluronidase (H3506; Sigma-Aldrich, St. Louis, MO), and protease inhibitor cocktail (Nacalai Tesque, Kyoto, Japan) for 25 to 30 minutes in a warm (37°C) water bath. Isolated islets were collected manually. Islets were maintained in RPMI-1640 supplemented with 10% (v/v) FBS, 0.1% (v/v) P/S, 50μM β-mercaptoethanol, 10mM HEPES, and 1mM sodium pyruvate at 37°C in 5% CO_2, 95% air.

qRT-PCR. MIN6 cells were homogenized in Sepasol-RNA I reagent (09379-55, Nacalai Tesque), and RNA was manually isolated by phenol-chloroform extraction and ethanol precipitation. RNA from isolated islets was prepared with the RNeasy Micro Kit (74004, QIAGEN, Hilden, Germany) according to the manufacturer's instructions. cDNA was synthesized with a Prime Script RT Reagent Kit (RR047A, Takara Bio Inc., Shiga, Japan). qRT-PCR was performed with SYBR Premix Ex TaqII (RR820A, Takara Bio Inc.) in an ABI 7300 thermal cycler (Applied Biosystems, Foster City, CA). All data were normalized to *Actb* or *Tbp*. The primers for this study are listed in Supplemental Table 1.

RNA-seq analysis. RNA was extracted with the RNeasy Micro Kit (74004, QIAGEN)

415 according to the manufacturer's instructions. For Figure 1 samples, sequencing libraries
416 were prepared with a NEBNext Ultra II Directional RNA Library Prep Kit (7765L, New
417 England Biolabs, Ipswich, MA), and samples were sequenced on an Illumina NextSeq
418 500 platform in 76bp single-end reads. For Figure 4 samples, sequencing libraries were
419 prepared with a NEBNext Ultra II RNA Library Prep Kit (E7770, New England Biolabs)
420 and samples were sequenced on an Illumina NovaSeq 6000 platform in 150bp paired-end
421 reads. For reanalysis of RNA-seq data of *db/db* mice islets (accession number: GSE
422 107489), raw RNA-seq data were downloaded from NCBI Sequence Read Archive and
423 converted to the fastq format with SRA-Tools (v2.10.9). Reads were trimmed for
424 universal Illumina adaptors with TrimGalore (v0.6.5)
425 (http://www.bioinfor5matics.babraham.ac.uk/projects/trim galore/) and then mapped to
426 GENCODE 36 genome sequence (for human) or M25 genome sequence (for mouse) with
427 HISAT2 (v2.2.1; ref. 54). Mapped reads were sorted and converted to a binary
428 alignment/map format with SAMtools (v1.11; ref. 55). Gene assembly and quantification
429 were performed with Stringtie (v2.1.4; ref. 56), and gene-level count matrixes were
430 generated with python script prepDE.py3
431 (http://ccb.jhu.edu/software/stringtie/dl/prepDE.py3). Differentially expressed genes
432 (DEGs) were determined with DESeq2 (v1.28.0; ref. 57). DEGs (adjusted p-value < 0.01)

were used for gene ontology analysis with David (v6.8; ref. 58, 59). Raw and processed RNA sequencing were deposited in the Gene Expression Omnibus (GEO) under accession number GSE202603.

Screening for hypoxia-induced genes associated with transcriptional repression. Hypoxia-induced genes were defined as genes with an adjusted p value of less than 0.05 and a fold change (hypoxia/normoxia) greater than 2 in DESeq2 outputs. To identify hypoxia-induced genes that are commonly listed in mouse and human islets and MIN6 cells and are related to transcriptional repression, DESeq2 outputs in each group were processed as follows: For human islets, human-to-mouse Ensembl gene identifiers (IDs) conversion was carried out with Ensembl BioMart; and for MIN6 cells and mouse islets, only genes with mouse Ensembl gene IDs that can be mapped to those in human were selected. After this gene IDs conversion and gene filtering, overlapped genes were determined. Genes associated with transcriptional repression were manually selected out of the overlapped genes based on gene ontology annotations against each gene (obtained from Ensembl BioMart).

GSEA. Gene set enrichment analysis was performed with GSEA (v4.03; ref. 60) for "pre-

451 ranked" analyses, with the fold change between normoxia samples and hypoxia samples
452 as the input. Mouse Ensembl IDs were converted to be compatible with the human
453 annotations of the MSigDB gene lists by using a Mouse ENSEMBL Gene ID to Human
454 Orthologs MSigDB.v7.4.chip.
455
456 **Western blotting.** Cells were lysed in RIPA buffer (50mM Tris-HCl [pH 8.0], 150mM
457 NaCl, 0.1% sodium dodecyl sulfate [SDS], 1% NP-40, 5mM EDTA, and 0.5% sodium
458 deoxycholate) with a protease inhibitor cocktail. Total proteins were separated by SDS
459 polyacrylamide gel electrophoresis, transferred to polyvinylidene difluoride membranes
460 (Immuno-P; Millipore, Bedford, MA) and then probed with the primary antibody. After
461 incubation with the horseradish peroxidase (HRP)-conjugated secondary antibodies, the
462 HRP signals were visualized by using Chemi-Lumi One Super (02230-30, Nacalai
463 Tesque) and a ChemiDocTM Imaging System (Bio-Rad Laboratories, Hercules, CA). The
464 primary antibodies used in this study were anti-β-actin antibody (M177-3, MBL), anti-
465 BHLHB2 antibody (H00008553-M01, Abnova), anti-MafA antibody (A300-611A,
466 Bethyl Laboratories, Montgomery, TX), anti-glyceraldehyde-3-phosphate dehydrogenase
467 (GAPDH) antibody (2118, Cell Signaling Technology, Danvers, MA), anti-HIF1α
468 antibody (NB100-479, Novus Biologicals, Centennial, CO), and anti-HIF1β antibody

(5537, Cell Signaling Technology).

Insulin secretion assay and insulin content in MIN6 cells. MIN6 cells were seeded in a 24-well plate. In Figures 3A, 3B, and 3D, cells were incubated in 20% or 5% O_2 for 24 hours before assay. Cells were pre-conditioned in low-glucose (2.2mM) Krebs-Ringer-bicarbonate HEPES (KRBH) buffer (120mM NaCl, 4.7mM KCl, 1.2mM KH_2PO_4, 2.4mM $CaCl_2$, 1.2mM $MgCl_2$, 20mM $NaHCO_3$, 10mM HEPES, and 0.5% (v/v) BSA) for 1 hour. Cells were washed once with low-glucose KRBH and incubated in low-glucose KRBH for 1 hour, and the supernatant was collected. Then, cells were stimulated in high-glucose (22mM) KRBH or low-glucose + KCl (30mM) KRBH for 1 hour, and the supernatant was collected. Next, cells were lysed in cell lysis buffer, and the protein concentration was measured with a Pierce BCA Protein Assay Kit (23225, Thermo Fisher Scientific, Waltham, MA) to normalize the insulin level. To measure insulin content, MIN6 cells were pelleted and resuspended in acid-ethanol (1.5% HCl in 70% EtOH), rotated overnight at 4°C and neutralized with 1M Tris-HCl (pH 7.5; 1:1). The insulin concentration was determined with a mouse insulin enzyme-linked immunosorbent assay (ELISA; TMB) kit (AKRIN-011T; Shibayagi Co., Ltd., Gunma, Japan). A hypoxia chamber glove box (Creative Bio Station: CBS-120; ASTEC) was used to achieve

487 continuous hypoxic conditions during the assay.

488

489 **Insulin secretion assay in mouse islets.** The islets isolated from Ctrl and βB40KO mice
490 were cultured in 5% O_2 for 24 hours. Then, they were preincubated for 30 minutes in
491 KRBH buffer containing 2.2mM glucose. For glucose challenge, they were incubated in
492 KRBH buffer containing 2.2mM or 22mM glucose for 30 minutes, and the supernatant
493 was collected; and for KCl challenge, they were incubated in KRBH buffer containing
494 2.2mM or 2.2mM glucose plus 30mM KCl for 30 minutes, and the supernatant was
495 collected. The insulin concentration was determined with a mouse insulin ELISA (TMB)
496 kit (AKRIN-011T and AKRIN-011S; Shibayagi Co., Ltd.). A hypoxia chamber glove box
497 (Creative Bio Station: CBS-120; ASTEC) was used to achieve continuous hypoxic
498 conditions during the assay.

499

500 **Cell proliferation assay.** Before the assay, Ctrl or *Bhlhe40* KD MIN6 cells were seeded
501 in a 96-well plate at 2 x 10^4 cells/well, incubated overnight and transferred to 20% or 5%
502 O_2. Cells were counted at 0, 24, 48, and 96 hours with a Cell Counting Kit-8 (343-07623,
503 Dojindo, Kumamoto, Japan), and the absorbance (450/655) was measured by an iMark
504 microplate reader (Bio-Rad Laboratories).

505

506 **Cell death assay.** Before the assay, Ctrl or *Bhlhe40* KD MIN6 cells were transferred to
507 and cultured in 20% or 5% O_2 for 24 hours. Then, they were incubated in 0.5 μg/ml PI
508 (341-07881, Dojindo) for 10 minutes, after which flow cytometric analyses were
509 performed with a FACSCalibur (BD Biosciences, Franklin Lakes, NJ) and FlowJo
510 software (Tomy Digital Biology, Tokyo, Japan).

511

512 **Calcium assay.** Ctrl or *Bhlhe40* OE MIN6 cells were plated on glass-bottomed culture
513 dishes (627871, Greiner Bio-One, Frickenhausen, Germany). The cells were preincubated
514 with KRBH buffer for 45 minutes and then incubated with KRBH buffer containing
515 2.2mM glucose, 2μM Fluo4-AM (F311, Dojindo), 0.02% Pluronic F-127 (P2443, Sigma-
516 Aldrich), 2.5mM probenecid (162-26112, Wako Pure Chemical Industries, Ltd.), and
517 Hochest 33258 (343-07961, Dojindo) for 30 minutes, after which the buffer was replaced
518 with dye-free KRBH buffer. To perform the KCl challenge, buffer was changed by hand-
519 aspirating it and gently adding an equal amount of KRBH buffer containing 2.2mM
520 glucose and 30mM KCl back into the dish with a micropipette Time-series images were
521 acquired every 10 seconds with a fluorescent microscope (BZ-X700; Keyence, Osaka,
522 Japan) and analyzed with Keyence software.

523

524 **hGH secretion assay.** Ctrl or *Bhlhe40* KD MIN6 were transfected with either pcDNA3-
525 empty or pcDNA3-hGH. At 24 hours after transfection, cells were transferred to and
526 cultured in 20% or 5% O_2 for a further 24 hours. Cells were preincubated in glucose-free
527 KRBH for 15 minutes and then incubated in KRBH with or without KCl (30mM) for 30
528 minutes, and the supernatant was collected. Cells were then lysed in cell lysis buffer, and
529 the protein concentration was measured with a Pierce BCA Protein Assay Kit (23225,
530 Thermo Fisher Scientific) to normalize the hGH level. The hGH concentration was
531 measured with Human Growth Hormone ELISA kit (ab190811, Abcam, Cambridge, UK).

532

533 **Glucose uptake assay.** Before the assay, Ctrl or *Bhlhe40* KD MIN6 cells were transferred
534 to and incubated in 20% or 5% O_2 for 24 hours. Cells were preincubated in KRBH for 15
535 minutes and then incubated in KRBH containing 200μM 2-NBDG (23002-v, Peptide
536 Institute, Inc., Osaka, Japan) plus 22mM glucose for 15 minutes, after which flow
537 cytometric analyses were performed with FACSCalibur (BD Biosciences) and FlowJo
538 software (Tomy Digital Biology).

539

540 **Mitochondrial mass assay.** Before the assay, Ctrl or *Bhlhe40* KD MIN6 cells were

transferred to and incubated in 20% or 5% O_2 for 24 hours. Then, cells were incubated in 2nM nonyl acridine orange (A-1372, Invitrogen, Carlsbad, CA) for 15 minutes, after which flow cytometric analyses were performed with FACSCalibur (BD Biosciences) and FlowJo software (Tomy Digital Biology).

Luciferase assay. MIN6 cells were transiently transfected with firefly luciferase plasmid (either pGL3-basic-MafA or its derivatives) and renilla luciferase plasmid (pRL-SV40) with jetPRIME transfection reagent (114-15, Polyplus). For *Bhlhe40* overexpression experiments, Bhlhe40 expression plasmids (either pcDNA3.1-empty or pcDNA3.1-Bhlhe40) were additionally transfected. Forty-eight hours after transfection, cells were lysed and assayed with firefly luciferase and renilla luciferase substrates in the Dual-Luciferase Reporter Assay System (E1980, Promega). Firefly luciferase activity (RLU1) was normalized to renilla luciferase activity (RLU2). For hypoxia experiments, cells were transferred to 20% or 5% O_2 for 24 hours before the luciferase activities were measured.

ChIP assay. MIN6 cells were fixed in 1% formaldehyde for 10 minutes at room temperature, and then the reaction was quenched by 150mM glycine for 5 minutes. The fixed cells were incubated in 0.5% Nonidet P-40 lysis buffer for 15 minutes on ice, and

559 the nuclei were pelleted and incubated in SDS lysis buffer (50mM Tris-HCl [pH 8.0], 1%
560 SDS, 10mM EDTA). Chromatin was then sheared with a Bioruptor sonicator (C30010016,
561 Diagenode, Seraing, Belgium) by 10 cycles of sonication at 30 seconds on, 30 seconds
562 off. The sheared chromatin was diluted 5-fold in ChIP dilution buffer (50mM Tris-HCl
563 [pH 8.0], 167mM NaCl, 1.1% Triton X-100, and 0.11% sodium deoxycholate) and then
564 incubated in Dynabeads protein A (1001D, Invitrogen) and protein G (1003D, Invitrogen)
565 for 1 hour at 4℃. After removing the beads, the chromatin was incubated in 4 μg of anti-
566 Bhlhe40 antibody (NB100-1800, Novus Biologicals) or control IgG (2729, Cell Signaling
567 Technology) overnight at 4℃. The antibody-protein complexes were isolated by
568 incubation with magnetic beads (Invitrogen Dynabeads protein A and protein G) for 6
569 hours at 4℃. Then, samples were sequentially washed with low-salt RIPA buffer (50mM
570 Tris-HCl [pH 8.0], 150mM NaCl, 1mM EDTA, 0.1% SDS, 1% Triton X-100, and 0.1%
571 sodium deoxycholate), high-salt RIPA buffer (50mM Tris-HCl [pH 8.0], 500mM NaCl,
572 1mM EDTA, 0.1% SDS, 1% Triton X-100, and 0.1% sodium deoxycholate), LiCl wash
573 buffer (10mM Tris-HCL [pH 8.0], 250mM LiCl, 1mM EDTA, 0.5% Nonidet P-40, and
574 0.5% sodium deoxycholate), and Tris-EDTA buffer and finally eluted and reversely cross-
575 linked in ChIP direct elution buffer (50mM Tris-HCl [pH 8.0], 5mM EDTA, and 0.5%
576 SDS) overnight at 65℃. DNA was then extracted and collected by phenol-chloroform

577 extraction and ethanol precipitation. DNA was amplified by qRT-PCR with SYBR Premix
578 Ex Taq II (RR820A, Takara) in ABI 7300 thermal cycler (Applied Biosystems) with the
579 primers listed in Supplemental Table 1.
580
581 **Metabolic analysis of mice.** Male 6- to 12-week-old mice were used for metabolic
582 analysis. For the glucose tolerance test, mice were fasted overnight. After intraperitoneal
583 glucose administration (2 g/kg for wildtype background, 1 g/kg for *ob/ob* background),
584 blood glucose levels were measured at 0, 15, 30, 60, 90, and 120 minutes. For the insulin
585 tolerance test, mice were fasted for 4 hours. After intraperitoneal insulin administration
586 (1 unit/kg for wildtype background, 3 units/kg for *ob/ob* background), blood glucose
587 levels were measured at 0, 30, 60, 90, and 120 minutes. For the glucose-stimulated insulin
588 secretion assay, mice were fasted overnight. After intraperitoneal administration of 3 g/kg
589 glucose, blood samples were collected at 0 and 15 minutes. The plasma insulin level was
590 determined with a mouse insulin ELISA (TMB) kit (AKRIN-011S; Shibayagi Co., Ltd.).
591
592 **Immunohistochemistry and β-cell mass assessment.** Pancreas tissues from mice were
593 fixed with 10% (v/v) neutral buffered formalin (060-01667, Wako Pure Chemical
594 Industries, Ltd.) for 16 to 18 hours at 4°C. Fixed samples were embedded in paraffin, cut

595 into 4-μm cross-sections, mounted on MAS-coated slides (Matsunami Glass, Osaka,
596 Japan). The deparaffinized sections were subjected to antigen retrieval (110℃, 20
597 minutes) with HistoVT One (L6F9587, Nacalai Tesque) and stained with the following
598 primary antibodies: anti-insulin antibody (A0564, 1:400; Dako, Santa Clara, CA), anti-
599 glucagon antibody (ab92517, 1:400; Abcam), anti-DEC1/BHLHE40 antibody (NB100-
600 1800, 1:100; Novus Biologicals), and anti-MafA antibody (A300-611A, 1:100; Bethyl
601 Laboratories). After reaction with fluorescent dye-conjugated secondary antibodies,
602 fluorescent signals were captured with an all-in-one fluorescent microscope (BZ-X700;
603 Keyence). The total islet area (μm^2) composed of insulin- and glucagon-stained cells was
604 measured by Keyence software, and the ratio of the total islet area to the total pancreas
605 area was calculated.
606
607 **Statistics.** The significance of differences was assessed by unpaired two-sided Student's
608 *t* tests, unless stated otherwise. All data are presented as means ± SEM. No statistical
609 analysis was used to predetermine the sample size.
610
611 **Study approval.** The handling and killing of mice were performed in compliance with
612 the animal care guidelines of Kumamoto University. All animal experiments were

conducted in accordance with the guidelines of the Institutional Animal Committee of Kumamoto University and were approved by the Kumamoto University Ethics Review Committee for Animal Experimentation (ID: A29-001, A 2019-048, A 2021-001). Human islets experiments were approved by the Ethical Committee of Kumamoto University Graduate School of Medical Sciences (No. 2389).

AUTHOR CONTRIBUTIONS

T.T., Y.S. and K.Y. conceived and designed the work; T.T. and Y.S. obtained the data; T.T., Y.S., T.Y., T.M., and K.Y. analyzed the data; T.T., Y.S. and K.Y. drafted the manuscript; All authors reviewed the results and approved the final version of the manuscript.

ACKNOWLEDGEMENT

We thank Dr. Douglas A. Melton (Harvard University) for providing Pdx1-Cre mice and Dr. Shingo Usuki (Kumamoto University) for his technical support. We also thank the members of Dr. Yamagata's laboratory for their technical assistance and discussions. This study was supported by Grants-in-Aid for Scientific Research (B) (19H03711 and 22H03129; K.Y.), by a Grant-in-Aid for Challenging Research (Exploratory) (19K22639; K.Y.), and by a Grant-in-Aid for Scientific Research (C) (19K09008; Y.S.); by grants from

631 the Takeda Science Foundation (K.Y. and Y.S.); and by grants from the program for
632 Leading Graduate Schools HIGO (T.T.) and Center for Metabolic Regulation of Healthy
633 Aging (T.T.).

634

635 **REFERENCES**

636 1. Prentki, M., Nolan, C.J. Islet beta cell failure in type 2 diabetes. *J Clin Invest*.
637 2006;116(7): 1802-12.

638

639 2. Kahn, S.E. et al. Pathophysiology and treatment of type 2 diabetes: perspectives on
640 the past, present, and future. *Lancet*. 2014;383(9922):1068-83.

641

642 3. Hudish, L.I. et al. β Cell dysfunction during progression of metabolic syndrome to
643 type 2 diabetes. *J Clin Invest*. 2019;129(10):4001-4008.

644

645 4. Sato, Y. et al. Cellular hypoxia of pancreatic beta-cells due to high levels of oxygen
646 consumption for insulin secretion in vitro. *J Biol Chem*. 2011;286(14):12524-32.

647

648 5. Bensellam, M. et al. Glucose-induced O_2 consumption activates hypoxia inducible

649 factors 1 and 2 in rat insulin-secreting pancreatic beta-cells. *PLoS One*
650 2012;7(1):e29807.
651
652 6. Zheng, X. et al. Acute hypoxia induces apoptosis of pancreatic β-cell by activation
653 of the unfolded protein response and upregulation of CHOP. *Cell Death Dis*.
654 2012;3(6): e322.
655
656 7. Ilegems, E. et al. HIF-1α inhibitor PX-478 preserves pancreatic β cell function in
657 diabetes. *Sci Transl Med*. 2022;14(638):eaba9112.
658
659 8. Kitamura, T. The role of FOXO1 in β-cell failure and type 2 diabetes mellitus. *Nat*
660 *Rev Endocrinol*. 2013;9(10):615-23.
661
662 9. Sato, Y. et al. Moderate hypoxia induces β-cell dysfunction with HIF-1-independent
663 gene expression changes. *PLoS One*. 2014;9(12):e114868.
664
665 10. Gerber, P.A., Rutter, G.A. The Role of Oxidative Stress and Hypoxia in Pancreatic
666 Beta-Cell Dysfunction in Diabetes Mellitus. *Antioxid Redox Signal*. 2017;26(10):501-

518.

11. Catrina, S.B., Zheng, X. Hypoxia and hypoxia-inducible factors in diabetes and its complications. *Diabetologia*. 2021;64(4):709-716.

12. Lee, P. et al. Cellular adaptation to hypoxia through hypoxia inducible factors and beyond. *Nat Rev Mol Cell Biol*. 2020;21(5):268-283.

13. Gunton, J.E. Hypoxia-inducible factors and diabetes. *J Clin Invest*. 2020;130(10):5063-5073.

14. Zehetner, J. et al. pVHL is a regulator of glucose metabolism and insulin secretion in pancreatic β cells. *Genes Dev*. 2008;22(22):3135-46.

15. Cantley, J. et al. Deletion of the von Hippel-Lindau gene in pancreatic beta cells impairs glucose homeostasis in mice. *J Clin Invest*. 2009;119(1):125-35.

16. Puri, S. et al. A role for von Hippel-Lindau protein in pancreatic beta-cell function.

685 *Diabetes*. 2009;58(2):433-41.

686

687 17. Cavadas, M.A.S. et al. The regulation of transcriptional repression in hypoxia. *Exp*
688 *Cell Res*. 2017;356(2):173-181.

689

690 18. St-Pierre, B. et al. Stra13 homodimers repress transcription through class B E-box
691 elements. *J Biol Chem*. 2002;277(48):46544-51.

692

693 19. Görlach, A. et al. Reactive oxygen species, nutrition, hypoxia and diseases: Problems
694 solved? *Redox Biol*. 2015;6:372-385.

695

696 20. Sato, Y. et al. Hypoxia reduces HNF4α/MODY1 protein expression in pancreatic β-
697 cells by activating AMP-activated protein kinase. *J Biol Chem*. 2017;292(21):8716-
698 8728.

699

700 21. Yun, Z. et al. Inhibition of PPAR gamma 2 gene expression by the HIF-1-regulated
701 gene DEC1/Stra13: a mechanism for regulation of adipogenesis by hypoxia. *Dev Cell*.
702 2002;2(3):331-41.

22. Miyazaki, K. et al. Identification of functional hypoxia response elements in the promoter region of the DEC1 and DEC2 genes. *J Biol Chem*. 2002;277(49):47014-21.

23. Ivanova, A. et al. STRA13 expression and subcellular localisation in normal and tumour tissues: implications for use as a diagnostic and differentiation marker. *J Med Genet*. 2005;42(7):565-76.

24. Sato, F. et al. DEC1 and DEC2 Crosstalk between Circadian Rhythm and Tumor Progression. *J Cancer*. 2016;7(2):153-9.

25. Rorsman, P., Renström, E. Insulin granule dynamics in pancreatic beta cells. *Diabetologia*. 2003;46(8):1029-45.

26. Coppola, T. et al. Disruption of Rab3-calmodulin interaction, but not other effector interactions, prevents Rab3 inhibition of exocytosis. *EMBO J*. 1999;18(21):5885-91.

721 27. Fukui, K. et al. The HNF-1 target collectrin controls insulin exocytosis by SNARE
722 complex formation. *Cell Metab*. 2005;2(6):373-84.
723
724 28. Hang, Y. et al. The MafA transcription factor becomes essential to islet β-cells soon
725 after birth. *Diabetes*. 2014;63(6):1994-2005.
726
727 29. Cataldo, L.R. et al. MAFA and MAFB regulate exocytosis-related genes in human β-
728 cells. *Acta Physiol (Oxf)*. 2022;234(2):e13761.
729
730 30. Oh, E. et al. Munc18-1 regulates first-phase insulin release by promoting granule
731 docking to multiple syntaxin isoforms. *J Biol Chem*. 2012;287(31):25821-33.
732
733 31. Nagamatsu, S. et al. alpha-soluble N-ethylmaleimide-sensitive factor attachment
734 protein is expressed in pancreatic beta cells and functions in insulin but not gamma-
735 aminobutyric acid secretion. *J Biol Chem*. 1999;274(12):8053-60.
736
737 32. Dolai, S. et al. Synaptotagmin-7 Functions to Replenish Insulin Granules for
738 Exocytosis in Human Islet β-Cells. *Diabetes*. 2016;65(7):1962-76.

739

740 33. Ohara-Imaizumi, M. et al. Imaging analysis reveals mechanistic differences between
741 first- and second-phase insulin exocytosis. *J Cell Biol*. 2007;177(4):695-705.

742

743

744 34. Zhang, C. et al. MafA is a key regulator of glucose-stimulated insulin secretion. *Mol*
745 *Cell Biol*. 2005;25(12):4969-76.

746

747 35. Puigserver, P., Spiegelman, B.M. Peroxisome proliferator-activated receptor-gamma
748 coactivator 1 alpha (PGC-1 alpha): transcriptional coactivator and metabolic regulator.
749 *Endocr Rev*. 2003;24(1):78-90.

750

751 36. LaGory, E.L. et al. Suppression of PGC-1α Is Critical for Reprogramming Oxidative
752 Metabolism in Renal Cell Carcinoma. *Cell Rep*. 2015;12(1):116-127.

753

754 37. Chung, S.Y. et al. Bhlhe40 Represses PGC-1α Activity on Metabolic Gene Promoters
755 in Myogenic Cells. *Mol Cell Biol*. 2015;35(14):2518-29.

756

38. Raum, J.C. et al. FoxA2, Nkx2.2, and PDX-1 regulate islet beta-cell-specific mafA expression through conserved sequences located between base pairs -8118 and -7750 upstream from the transcription start site. *Mol Cell Biol*. 2006;26(15):5735-43.

39. Yamamoto, K. et al. A novel function of Onecut1 protein as a negative regulator of MafA gene expression. *J Biol Chem*. 2013;288(30):21648-58.

40. Mathelier, A. et al. JASPAR 2016: a major expansion and update of the open-access database of transcription factor binding profiles. *Nucleic Acids Res*. 2016;44(D1):D110-5.

41. Sun, H., Taneja, R. Stra13 expression is associated with growth arrest and represses transcription through histone deacetylase (HDAC)-dependent and HDAC-independent mechanisms. *Proc Natl Acad Sci U S A*. 2000;97(8):4058-63.

42. Ivanova, A.V. et al. STRA13 interacts with STAT3 and modulates transcription of STAT3-dependent targets. *J Mol Biol*. 2004;340(4):641-53.

775 43. Raum, J.C. et al. Islet beta-cell-specific MafA transcription requires the 5'-flanking
776 conserved region 3 control domain. *Mol Cell Biol*. 2010;30(17):4234-44.
777
778 44. Skarnes, W.C. et al. A conditional knockout resource for the genome-wide study of
779 mouse gene function. *Nature*. 2011;474(7351):337-42.
780
781 45. Hsiao, S.P. et al. P/CAF rescues the Bhlhe40-mediated repression of MyoD
782 transactivation. *Biochem J*. 2009;422(2):343-52.
783
784 46. Gaston, K., Jayaraman, P.S. Transcriptional repression in eukaryotes: repressors and
785 repression mechanisms. *Cell Mol Life Sci*. 2003;60(4):721-41.
786
787 47. Jarjour, N.N. et al. Bhlhe40 mediates tissue-specific control of macrophage
788 proliferation in homeostasis and type 2 immunity. *Nat Immunol*. 2019;20(6):687-700.
789
790 48. Lin, J. et al. Metabolic control through the PGC-1 family of transcription coactivators.
791 *Cell Metab*. 2005;1(6):361-70.
792

793 49. Ling, C. et al. Epigenetic regulation of PPARGC1A in human type 2 diabetic islets
794 and effect on insulin secretion. *Diabetologia*. 2008;51(4):615-22.
795
796 50. Li, D. et al. The repression of IRS2 gene by ATF3, a stress-inducible gene, contributes
797 to pancreatic beta-cell apoptosis. *Diabetes*. 2008;57(3):635-44.
798
799 51. Ku, H.C., Cheng, C.F. Master Regulator Activating Transcription Factor 3 (ATF3) in
800 Metabolic Homeostasis and Cancer. *Front Endocrinol (Lausanne)*. 2020;11:556.
801
802 52. Nishiyama, Y. et al. HIF-1α induction suppresses excessive lipid accumulation in
803 alcoholic fatty liver in mice. *J Hepatol*. 2012;56(2):441-7.
804
805 53. Shen, L. et al. Hepatic differentiated embryo-chondrocyte-expressed gene 1 (Dec1)
806 inhibits sterol regulatory element-binding protein-1c (Srebp-1c) expression and
807 alleviates fatty liver phenotype. *J Biol Chem*. 2014;289(34):23332-42.
808
809 54. Kim, D. et al. Graph-based genome alignment and genotyping with HISAT2 and
810 HISAT-genotype. *Nat Biotechnol*. 2019;37(8):907-915.

811

812 55. Li, H. et al. The Sequence Alignment/Map format and SAMtools. *Bioinformatics*.
813 2009;25(16):2078-9.

814

815 56. Pertea, M. et al. StringTie enables improved reconstruction of a transcriptome from
816 RNA-seq reads. *Nat Biotechnol*. 2015;33(3):290-5.

817

818 57. Love, M. I. et al. Moderated estimation of fold change and dispersion for RNA-seq
819 data with DESeq2. *Genome Biology*. 2014;15(12):550.

820

821 58. Huang, W. et al. Bioinformatics enrichment tools: paths toward the comprehensive
822 functional analysis of large gene lists. *Nucleic Acids Res*. 2009;37(1):1-13.

823

824 59. Huang W. et al. Systematic and integrative analysis of large gene lists using DAVID
825 bioinformatics resources. *Nat Protoc*. 2009;4(1):44-57.

826

827 60. Subramanian, A. et al. Gene set enrichment analysis: a knowledge-based approach for
828 interpreting genome-wide expression profiles. *Proc Natl Acad Sci U S A*.

2005;102(43):15545-50.

FIGURES

Figure 1. Global gene expression in hypoxic β-cells and islets. (**A**) Heatmap of β-cell genes in mouse islets (20% vs 5% O_2 for 24 hours; n = 3) and human islets (20% [n = 2] or 2% [n = 3] O_2 for 24 hours). (**B**) Gene set enrichment analysis of mouse islets (20% vs 5% O_2 for 24 hours; n = 3) and human islets (20% [n = 2] or 2% [n = 3] O_2 for 24 hours). (**C**) RNA-seq data of hypoxia-induced genes in mouse islets (20% vs 5% O_2 for 24 hours; n = 3), human islets (20% [n = 2] vs 2% [n = 3] O_2 for 24 hours), and MIN6 cells (20% vs 5% O_2 for 6 hours; n = 3). The Venn diagram shows the coordinated elevation of 25 genes, two of which (*Atf3* and *Bhlhe40*) are associated with transcriptional repression. (**D**-**F**) Volcano plots showing RNA-seq data in mouse islets (20% vs 5% O_2 for 24 hours; n = 3; **D**), human islets (20% [n = 2] vs 2% [n = 3] O_2 for 24 hours; **E**), and MIN6 cells (20% vs 5% O_2 for 6 hours; n = 3; **F**). *Atf3*, *Bhlhe40*, and other reported hypoxia-inducible transcriptional repressor genes (17) are shown (red, significantly upregulated genes).

Figure 2. BHLHE40 expression and its regulation in hypoxic β-cells and islets. (**A**-**C**) Western blots of BHLHE40 expression across tissues (**A**), BHLHE40 expression in

MIN6 cells cultured under 20% or 5% O_2 for the indicated time (**B**), and BHLHE40 expression in mouse islets cultured under 20% or 5% O_2 for 24 hours (**C**). (**D-F**) The effect of oxidative stress, endoplasmic reticulum stress, and energy stress on BHLHE40 expression. qRT-PCR analysis of *Bhlhe40* in MIN6 cells incubated with 10μM H_2O_2 (n = 3; **D**), 2μM thapsigargin (Thap) or 5 μg/ml tunicamycin (Tun) (n = 3; **E**), or 2mM metformin (Met) for 24 hours (n = 3; **F**). (**G**) The effect of short-hairpin RNA-mediated *Hif1β* knockdown (KD) on BHLHE40 expression in MIN6 cells cultured under 20% or 5% O_2 for 24 hours (n = 3). (**H-K**) BHLHE40 expression in islets from diabetic mice. BHLHE40 expression was analyzed in *ob/ob* mouse islets by qRT-PCR (n = 4; **H**) and Western blotting (**I**) and in *db/db* mouse islets by Western blotting (**J**). Subcellular localization of BHLHE40 in *ob/ob* mice islets by immunohistochemical analysis (**K**). Data are mean ± SEM; *p < 0.05 and ***p < 0.001 by unpaired two-tailed Student's *t* test. Glyceraldehyde-3-phosphate dehydrogenase (GAPDH) or β-actin was used as a loading control. Scale bar, 10 μm. HPT, hypothalamus; Ctrl, control; n.s., not significant.

Figure 3. BHLHE40 controls insulin secretion in β-cells. (**A**) Glucose-stimulated insulin secretion in MIN6 cells expressing short hairpin RNA against a non-targeting Ctrl or *Bhlhe40* knockdown (*B40* KD) were cultured under 20% or 5% O_2 for 24 hours (n =

865 8). (**B**) Insulin contents in MIN6 cells cultured under 20% or 5% O_2 for 24 hours (n = 3).
866 (**C**) Glucose-stimulated insulin secretion in MIN6 cells infected with retroviruses
867 generated with pMx-Ctrl (Ctrl) or pMx-*Bhlhe40* (*B40* OE; n = 4). (**D**) KCl-stimulated
868 insulin secretion in Ctrl and *B40* KD MIN6 cells cultured under 20% or 5% O_2 for 24
869 hours (n = 4). (**E**) KCl-stimulated insulin secretion in Ctrl and *B40* OE MIN6 cells (n =
870 3). (**F-G**) Calcium influx stimulated by 30mM KCl in Ctrl and *B40* OE MIN6 cells (n =
871 70 cells from n = 3 biological replicates) (**F**) and the AUC of **F** (**G**). (**H**) hGH secretion
872 after stimulation by 2.2mM glucose or 2.2mM glucose plus 30mM KCl in Ctrl and *B40*
873 KD MIN6 cells cultured under 20% or 5% O_2 for 24 hours (n = 3). (**I-K**) Glucose uptake
874 (n = 3; **I**), cellular ATP content (n = 4; **J**), and mitochondrial mass (n = 4 ;**K**) in Ctrl and
875 *B40* KD MIN6 cells cultured under 20% or 5% O_2 for 24 hours. Data are mean ± SEM;
876 *p < 0.05 and ***p < 0.001 by unpaired two-tailed Student's *t* test. Ctrl, control; n.s., not
877 significant.
878
879 **Figure 4. BHLHE40 suppresses *Mafa* expression in β-cells.** (**A**) MA plot of RNA-seq
880 data in Ctrl and *B40* OE MIN6 cells. Differentially expressed genes (DEGs; adjusted p
881 value < 0.01) are shown in blue, and others in gray. DEGs functioning as β-cell
882 transcription factors are shown in red (n = 3). (**B**) Gene ontology analysis of RNA-seq

data. Downregulated DEGs were used as input. (**C** and **D**) Expression of DEGs shown in **A** was confirmed by qRT-PCR in Ctrl and *B40* OE MIN6 cells (n = 3; **C**) or Ctrl and *B40* KD MIN6 cells cultured under 20% or 5% O_2 for 24 hours (n = 3; **D**). (**E**-**F**) Western blot of BHLHE40 and MAFA expression in Ctrl and *B40* OE MIN6 cells (**E**) or Ctrl and *B40* KD MIN6 cells cultured under 20% or 5% O_2 for 24 hours (**F**). (**G**) qRT-PCR of MAFA target genes in Ctrl and *B40* KD MIN6 cells cultured under 20% or 5% O_2 for 24 hours (n = 3). (**H**) Glucose-stimulated insulin secretion in MIN6 cells infected with AAV-green fluorescent protein (GFP) (Ctrl) or AAV-*Mafa* and cultured under 20% or 5% O_2 for 24 hours (n = 4). (**I**) KCl-stimulated insulin secretion in MIN6 cells infected with AAV-GFP (Ctrl) and AAV-*Mafa* and cultured under 20% or 5% O_2 for 24 hours (n = 4). Data are mean ± SEM; *p < 0.05, *p < 0.01 and ***p < 0.001 by unpaired two-tailed Student's *t* test. β-actin was used as a loading control. Ctrl, control.

Figure 5. BHLHE40 controls *Mafa* expression via two E-box sites in the enhancer region. (**A**) Reporter gene analysis with luciferase plasmid infused with mouse MAFA promoter/enhancer (-10427/+22 bp from transcription start site) in Ctrl and *B40* KD MIN6 cells cultured under 20% or 5% O_2 for 24 hours (n = 4). (**B**) BHLHE40-binding motif (upper left) and JASPAR results (lower left) are presented. JASPAR predicted four

E-box sites for BHLHE40 binding on MAFA promoter/enhancer (relative score > 0.9, E-box sites are underlined). (**C**) Luciferase reporter assay was performed with MIN6 cells transfected with BHLHE40 expression plasmids, pRL-SV40 plasmid, and pGL3-Mafa plasmids (wildtype [black] and E-box mutated [red] sites; n = 4). (**D**) Luciferase reporter activity in MIN6 cells cultured under 20% or 5% O_2 for 24 hours (n = 3). (**E**) MIN6 cells were cultured in 20% or 5% O_2 for 24 hours, and then the proteins were immuno-precipitated by IgG or anti-BHLHE40 specific antibody, after which qRT-PCR was performed for the indicated regions (n = 3). (**F**) Luciferase reporter assay in MIN6 cells incubated with 0.1μM TSA or vehicle for 24 hours (n = 4). (**G**) Proteins sampled from Ctrl and *B40* OE MIN6 cells with FLAG-Pdx1 expression were immuno-precipitated by IgG or anti-FLAG antibody, after which qRT-PCR was performed for the indicated regions (n = 9). Data are mean ± SEM; *p < 0.05 **p < 0.01, and ***p < 0.001 by unpaired two-tailed Student's *t* test. Ctrl, control; n.s., not significant.

Figure 6. Deficiency of BHLHE40 improves hyperglycaemia in *ob/ob* mice. (**A**) Glucose tolerance test of *Pdx1*-Cre (*Cre*), *Bhlhe40*$^{fl/fl}$ (*B40*$^{fl/fl}$), and *Pdx1*-Cre:*Bhlhe40*$^{fl/fl}$ (*Cre:B40*$^{fl/fl}$) mice (n = 7, n = 12, and n = 9 respectively; 8-12 weeks old). (**B**) Body weight of *Bhlhe40*$^{fl/fl}$ (Ctrl):*ob/ob* and *Pdx1*-Cre:*Bhlhe40*$^{fl/fl}$ (βB40KO):*ob/ob* mice (n = 9 and n

= 6, respectively). (**C** and **D**) Glucose tolerance test of Ctrl:*ob/ob* and βB40KO:*ob/ob* mice (n = 9 and n = 8, respectively; 6 weeks old) (**C**) and AUC (**D**). (**E**) Glucose-stimulated insulin secretion in Ctrl:*ob/ob* and βB40KO:*ob/ob* mice (n = 9 and n = 6, respectively; 8 weeks old). (**F**) Glucose-stimulated insulin secretion in isolated islets from Ctrl and βB40KO mice after culture under 5% O_2 for 24 hours (n = 8). (**G**) KCl-stimulated insulin secretion in isolated islets from Ctrl and βB40KO mice after incubation with 5% O_2 for 24 hours (n = 8). (**H**) ATP content in isolated islets of Ctrl and βB40KO mice after incubation with 20% or 5% O_2 for 24 hours (n = 4). (**I** and **J**) Representative images of pancreatic islets stained for insulin and glucagon in Ctrl:*ob/ob* and βB40KO:*ob/ob* mice (12 weeks old) (**I**). The ratios of total islet area to whole pancreas area (%) are shown (n = 3; **J**). (**K** and **L**) Representative images of pancreatic islets stained for insulin, MAFA, and BHLHE40 in Ctrl:*ob/ob* and βB40KO:*ob/ob* mice (12 weeks old) (**K**). Fluorescence intensities of nuclear and cytosolic MAFA in **K** were quantified (n = 30; **L**). (**M**) qRT-PCR of *Mafa* and its target genes in Ctrl:*ob/ob* and βB40KO:*ob/ob* mice (n = 4). Data are mean ± SEM; *p < 0.05 **p < 0.01, and ***p < 0.001 by unpaired two-tailed Student's *t* test. Scale bar, 10 μm. Ctrl, control; n.s., not significant.

Figure 7. A proposed model for how hypoxia causes β-cells dysfunction.

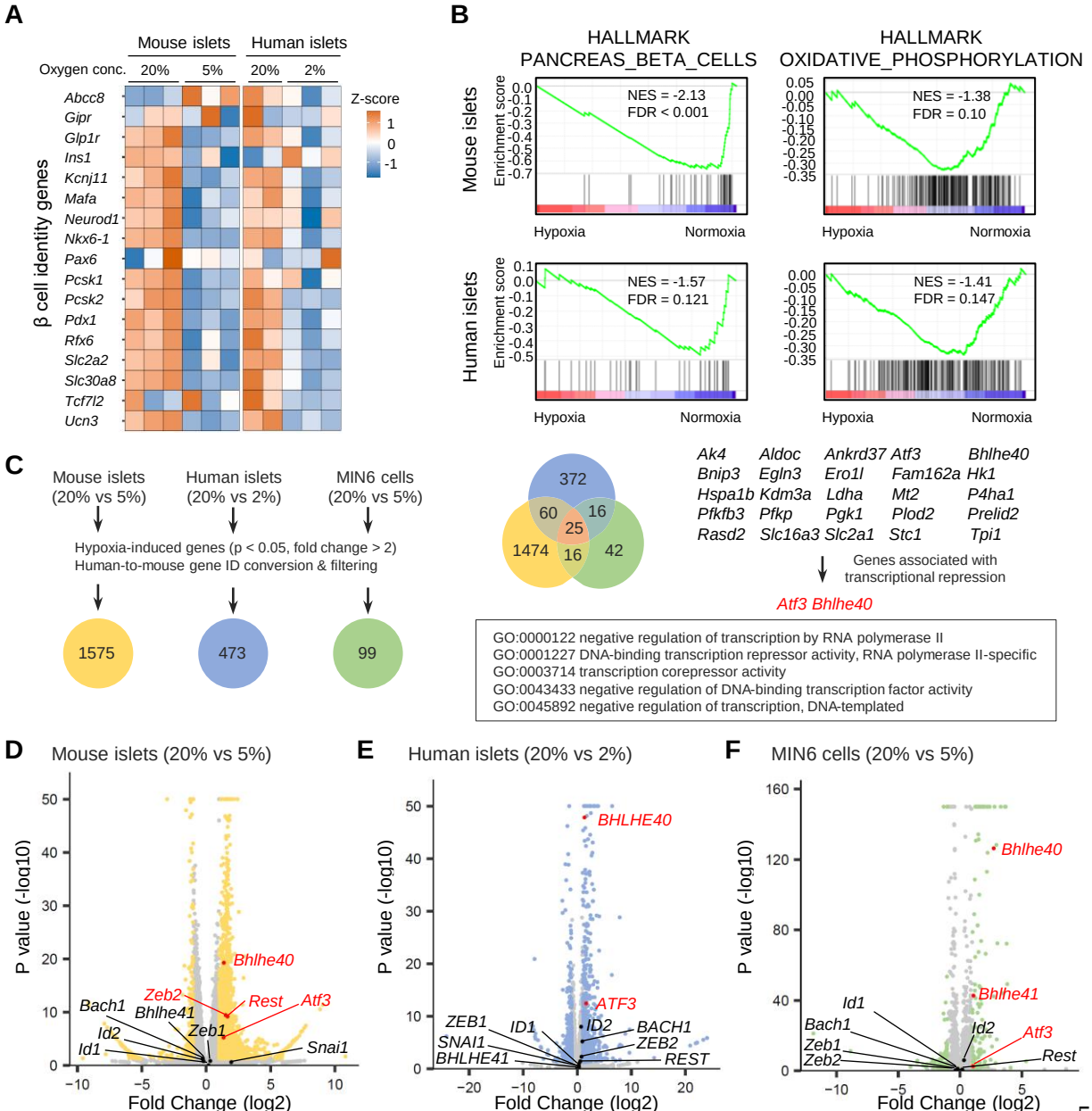
A
Mouse islets
Human islets
Oxygen conc.
20%
5%
20%
2%
Z-score
1
0
-1
β cell identity genes
Abcc8
Gipr
Glp1r
Ins1
Kcnj11
Mafa
Neurod1
Nkx6-1
Pax6
Pcsk1
Pcsk2
Pdx1
Rfx6
Slc2a2
Slc30a8
Tcf7l2
Ucn3
B
HALLMARK
PANCREAS_BETA_CELLS
HALLMARK
OXIDATIVE_PHOSPHORYLATION
Mouse islets
Human islets
Enrichment score
NES = -2.13
FDR < 0.001
NES = -1.38
FDR = 0.10
NES = -1.57
FDR = 0.121
NES = -1.41
FDR = 0.147
Hypoxia
Normoxia
C
Mouse islets
(20% vs 5%)
Human islets
(20% vs 2%)
MIN6 cells
(20% vs 5%)
Hypoxia-induced genes (p < 0.05, fold change > 2)
Human-to-mouse gene ID conversion & filtering
1575
473
99
372
60
16
25
1474
16
42
Ak4 Aldoc Ankrd37 Atf3 Bhlhe40
Bnip3 Egln3 Ero1l Fam162a Hk1
Hspa1b Kdm3a Ldha Mt2 P4ha1
Pfkfb3 Pfkp Pgk1 Plod2 Prelid2
Rasd2 Slc16a3 Slc2a1 Stc1 Tpi1
Genes associated with
transcriptional repression
Atf3 Bhlhe40
GO:0000122 negative regulation of transcription by RNA polymerase II
GO:0001227 DNA-binding transcription repressor activity, RNA polymerase II-specific
GO:0003714 transcription corepressor activity
GO:0043433 negative regulation of DNA-binding transcription factor activity
GO:0045892 negative regulation of transcription, DNA-templated
D
Mouse islets (20% vs 5%)
P value (-log10)
Fold Change (log2)
Bhlhe40
Zeb2
Rest
Atf3
Bach1
Bhlhe41
Id2
Zeb1
Id1
Snai1
E
Human islets (20% vs 2%)
BHLHE40
ATF3
ZEB1
ID1
ID2
BACH1
SNAI1
ZEB2
BHLHE41
REST
F
MIN6 cells (20% vs 5%)
Bhlhe40
Bhlhe41
Id1
Bach1
Id2
Atf3
Zeb1
Zeb2
Rest

Figure 1. Global gene expression in hypoxic β-cells and islets. (**A**) Heatmap of β-cell genes in mouse islets (20% vs 5% O_2 for 24 hours; n = 3) and human islets (20% [n = 2] or 2% [n = 3] O_2 for 24 hours). (**B**) Gene set enrichment analysis of mouse islets (20% vs 5% O_2 for 24 hours; n = 3) and human islets (20% [n = 2] or 2% [n = 3] O_2 for 24 hours). (**C**) RNA-seq data of hypoxia-induced genes in mouse islets (20% vs 5% O_2 for 24 hours; n = 3), human islets (20% [n = 2] vs 2% [n = 3] O_2 for 24 hours), and MIN6 cells (20% vs 5% O_2 for 6 hours; n = 3). The Venn diagram shows the coordinated elevation of 25 genes, two of which (*Atf3* and *Bhlhe40*) are associated with transcriptional repression. (**D**-**F**) Volcano plots showing RNA-seq data in mouse islets (20% vs 5% O_2 for 24 hours; n = 3; **D**), human islets (20% [n = 2] vs 2% [n = 3] O_2 for 24 hours; **E**), and MIN6 cells (20% vs 5% O_2 for 6 hours; n = 3; **F**). *Atf3*, *Bhlhe40*, and other reported hypoxia-inducible transcriptional repressor genes (17) are shown (red, significantly upregulated genes).

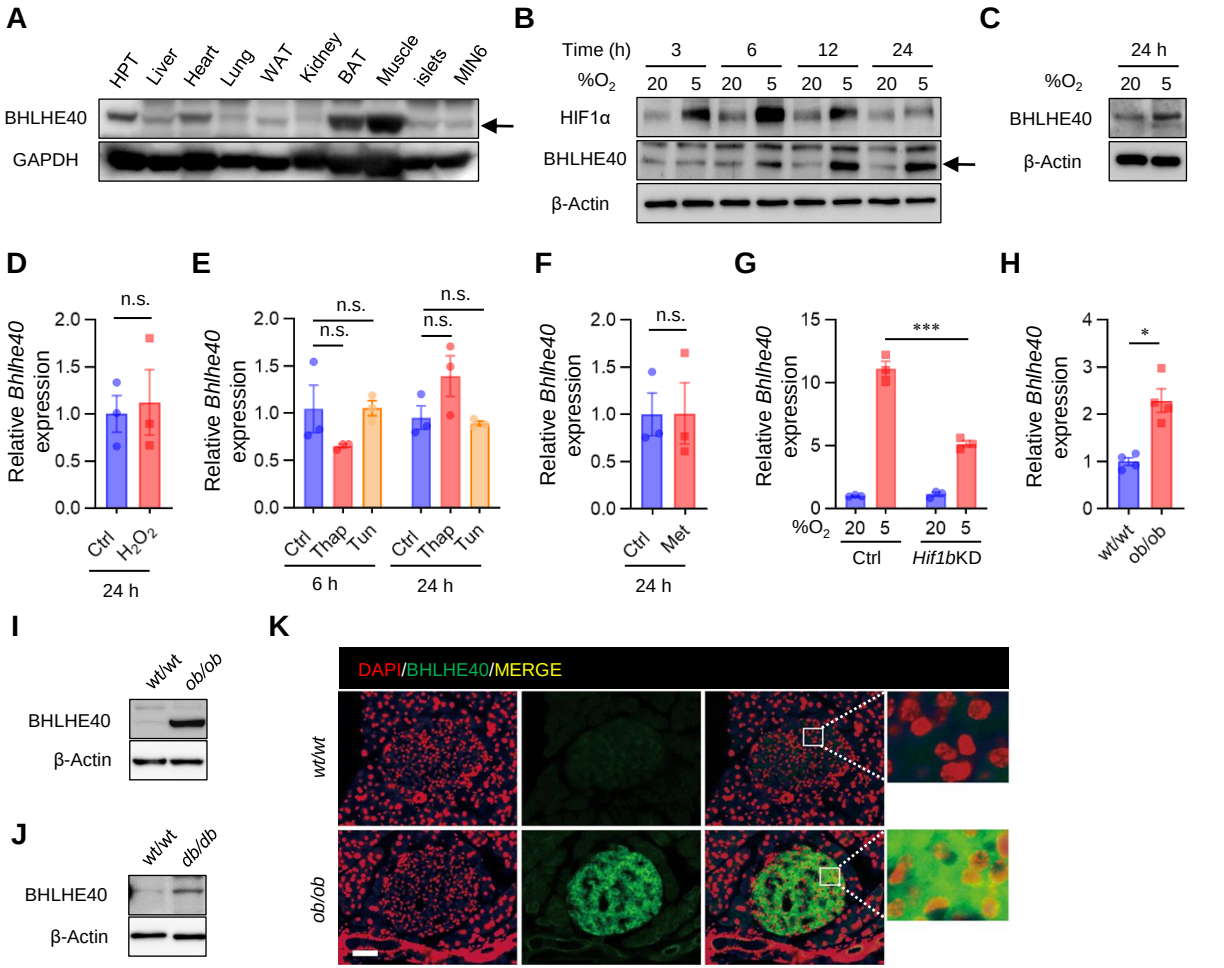
A
HPT
Liver
Heart
Lung
WAT
Kidney
BAT
Muscle
islets
MIN6
BHLHE40
GAPDH
B
Time (h)
3
6
12
24
%O2
20
5
HIF1α
BHLHE40
β-Actin
C
24 h
%O2
20
5
BHLHE40
β-Actin
D
Relative Bhlhe40 expression
n.s.
Ctrl
H2O2
24 h
E
Relative Bhlhe40 expression
n.s.
Ctrl
Thap
Tun
6 h
24 h
F
Relative Bhlhe40 expression
n.s.
Ctrl
Met
24 h
G
Relative Bhlhe40 expression
***
%O2
Ctrl
Hif1bKD
H
Relative Bhlhe40 expression
*
wt/wt
ob/ob
I
wt/wt
ob/ob
BHLHE40
β-Actin
J
wt/wt
db/db
BHLHE40
β-Actin
K
DAPI/BHLHE40/MERGE
wt/wt
ob/ob

Figure 2. BHLHE40 expression and its regulation in hypoxic β-cells and islets. (**A**-**C**) Western blots of BHLHE40 expression across tissues (**A**), BHLHE40 expression in MIN6 cells cultured under 20% or 5% O_2 for the indicated time (**B**), and BHLHE40 expression in mouse islets cultured under 20% or 5% O_2 for 24 hours (**C**). (**D**-**F**) The effect of oxidative stress, endoplasmic reticulum stress, and energy stress on BHLHE40 expression. qRT-PCR analysis of *Bhlhe40* in MIN6 cells incubated with 10μM H_2O_2 (n = 3; **D**), 2μM thapsigargin (Thap) or 5 μg/ml tunicamycin (Tun) (n = 3; **E**), or 2mM metformin (Met) for 24 hours (n = 3; **F**). (**G**) The effect of short-hairpin RNA-mediated *Hif1β* knockdown (KD) on BHLHE40 expression in MIN6 cells cultured under 20% or 5% O_2 for 24 hours (n = 3). (**H**-**K**) BHLHE40 expression in islets from diabetic mice. BHLHE40 expression was analyzed in *ob/ob* mouse islets by qRT-PCR (n = 4; **H**) and Western blotting (**I**) and in *db/db* mouse islets by Western blotting (**J**). Subcellular localization of BHLHE40 in *ob/ob* mice islets by immunohistochemical analysis (**K**). Data are mean ± SEM; *p < 0.05 and ***p < 0.001 by unpaired two-tailed Student's *t* test. Glyceraldehyde-3-phosphate dehydrogenase (GAPDH) or β-actin was used as a loading control. Scale bar, 10 μm. HPT, hypothalamus; Ctrl, control; n.s., not significant.

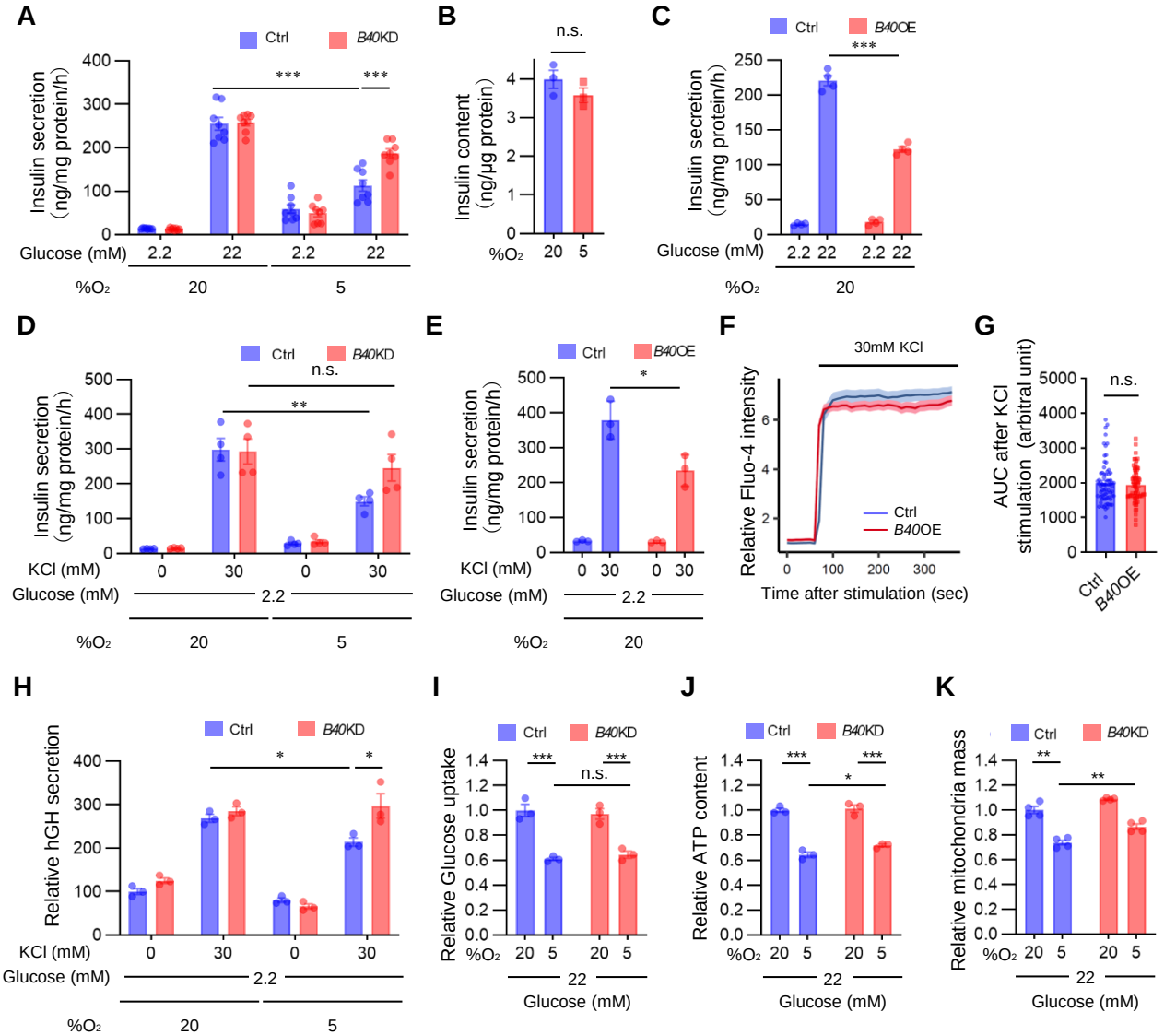
A
Ctrl
B40KD
Insulin secretion (ng/mg protein/h)
***
***
Glucose (mM)
2.2
22
2.2
22
%O2
20
5
B
n.s.
Insulin content (ng/μg protein)
%O2
20
5
C
Ctrl
B40OE
***
Insulin secretion (ng/mg protein/h)
Glucose (mM)
2.2
22
2.2
22
%O2
20
D
Ctrl
B40KD
n.s.
**
Insulin secretion (ng/mg protein/h)
KCl (mM)
0
30
0
30
Glucose (mM)
2.2
%O2
20
5
E
Ctrl
B40OE
*
Insulin secretion (ng/mg protein/h)
KCl (mM)
0
30
0
30
Glucose (mM)
2.2
%O2
20
F
30mM KCl
Relative Fluo-4 intensity
Ctrl
B40OE
Time after stimulation (sec)
G
n.s.
AUC after KCl stimulation (arbitral unit)
Ctrl
B40OE
H
Ctrl
B40KD
*
*
Relative hGH secretion
KCl (mM)
0
30
0
30
Glucose (mM)
2.2
%O2
20
5
I
Ctrl
B40KD
***
***
n.s.
Relative Glucose uptake
%O2
20
5
20
5
22
Glucose (mM)
J
Ctrl
B40KD
***
***
*
Relative ATP content
%O2
20
5
20
5
22
Glucose (mM)
K
Ctrl
B40KD
**
**
Relative mitochondria mass
%O2
20
5
20
5
22
Glucose (mM)

Figure 3. BHLHE40 controls insulin secretion in β-cells. (**A**) Glucose-stimulated insulin secretion in MIN6 cells expressing short hairpin RNA against a non-targeting Ctrl or *Bhlhe40* knockdown (*B40* KD) were cultured under 20% or 5% O_2 for 24 hours (n = 8). (**B**) Insulin contents in MIN6 cells cultured under 20% or 5% O_2 for 24 hours (n = 3). (**C**) Glucose-stimulated insulin secretion in MIN6 cells infected with retroviruses generated with pMx-Ctrl (Ctrl) or pMx-*Bhlhe40* (*B40* OE; n = 4). (**D**) KCl-stimulated insulin secretion in Ctrl and *B40* KD MIN6 cells cultured under 20% or 5% O_2 for 24 hours (n = 4). (**E**) KCl-stimulated insulin secretion in Ctrl and *B40* OE MIN6 cells (n = 3). (**F-G**) Calcium influx stimulated by 30mM KCl in Ctrl and *B40* OE MIN6 cells (n = 70 cells from n = 3 biological replicates) (**F**) and the AUC of **F** (**G**). (**H**) hGH secretion after stimulation by 2.2mM glucose or 2.2mM glucose plus 30mM KCl in Ctrl and *B40* KD MIN6 cells cultured under 20% or 5% O_2 for 24 hours (n = 3). (**I-K**) Glucose uptake (n = 3; **I**), cellular ATP content (n = 4; **J**), and mitochondrial mass (n = 4 ;**K**) in Ctrl and *B40* KD MIN6 cells cultured under 20% or 5% O_2 for 24 hours. Data are mean ± SEM; *p < 0.05 and ***p < 0.001 by unpaired two-tailed Student's *t* test. Ctrl, control; n.s., not significant.

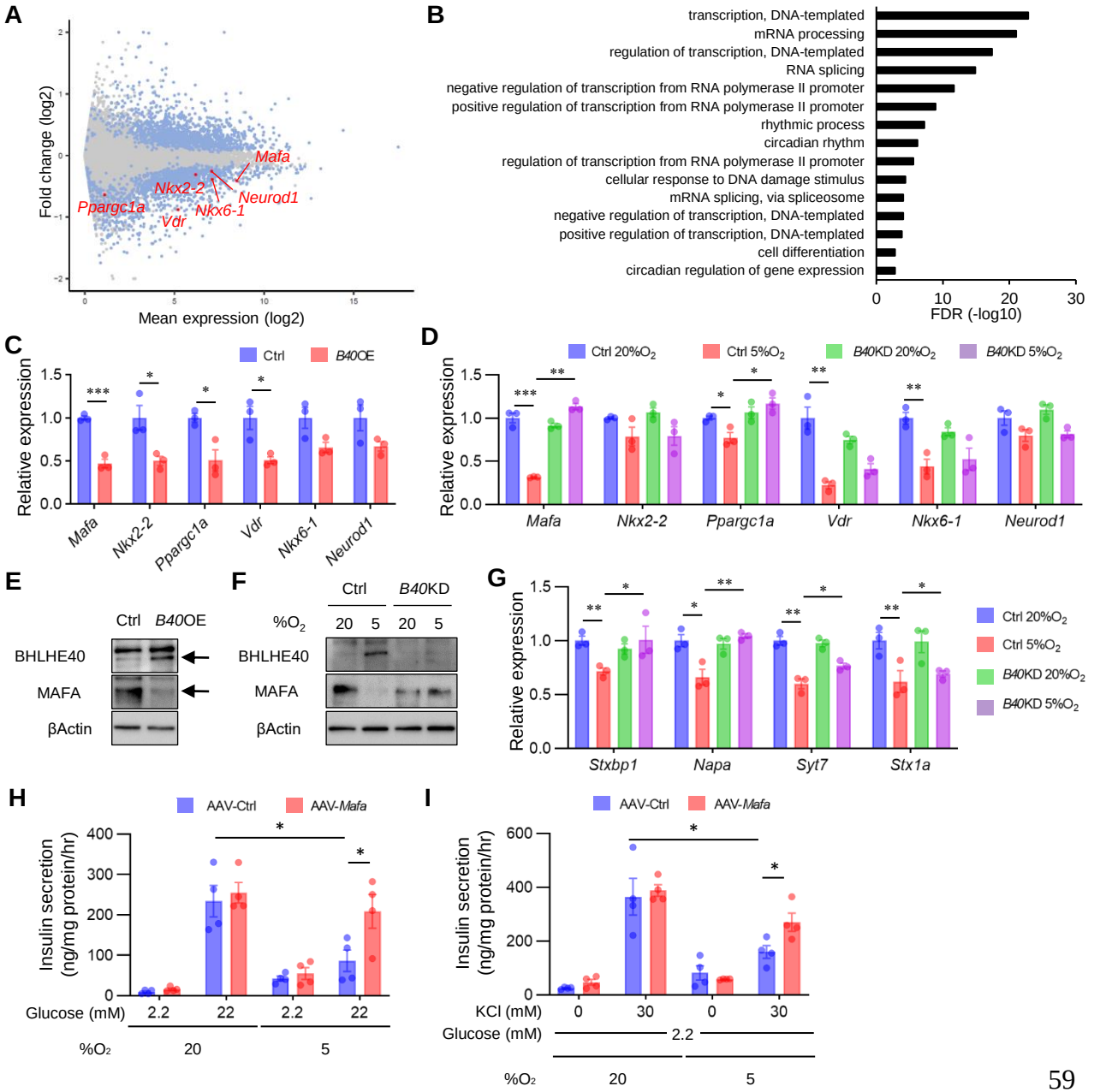
A
Fold change (log2)
Mean expression (log2)
Mafa
Nkx2-2
Neurod1
Ppargc1a
Nkx6-1
Vdr
B
transcription, DNA-templated
mRNA processing
regulation of transcription, DNA-templated
RNA splicing
negative regulation of transcription from RNA polymerase II promoter
positive regulation of transcription from RNA polymerase II promoter
rhythmic process
circadian rhythm
regulation of transcription from RNA polymerase II promoter
cellular response to DNA damage stimulus
mRNA splicing, via spliceosome
negative regulation of transcription, DNA-templated
positive regulation of transcription, DNA-templated
cell differentiation
circadian regulation of gene expression
FDR (-log10)
C
Ctrl
B40OE
Relative expression
Mafa
Nkx2-2
Ppargc1a
Vdr
Nkx6-1
Neurod1
D
Ctrl 20%O2
Ctrl 5%O2
B40KD 20%O2
B40KD 5%O2
Relative expression
Mafa
Nkx2-2
Ppargc1a
Vdr
Nkx6-1
Neurod1
E
Ctrl
B40OE
BHLHE40
MAFA
βActin
F
Ctrl
B40KD
%O2
20
5
20
5
BHLHE40
MAFA
βActin
G
Relative expression
Stxbp1
Napa
Syt7
Stx1a
Ctrl 20%O2
Ctrl 5%O2
B40KD 20%O2
B40KD 5%O2
H
AAV-Ctrl
AAV-Mafa
Insulin secretion (ng/mg protein/hr)
Glucose (mM)
2.2
22
2.2
22
%O2
20
5
I
AAV-Ctrl
AAV-Mafa
Insulin secretion (ng/mg protein/hr)
KCl (mM)
0
30
0
30
Glucose (mM)
2.2
%O2
20
5

Figure 4. BHLHE40 suppresses *Mafa* expression in β-cells. (**A**) MA plot of RNA-seq data in Ctrl and *B40* OE MIN6 cells. Differentially expressed genes (DEGs; adjusted p value < 0.01) are shown in blue, and others in gray. DEGs functioning as β-cell transcription factors are shown in red (n = 3). (**B**) Gene ontology analysis of RNA-seq data. Downregulated DEGs were used as input. (**C** and **D**) Expression of DEGs shown in **A** was confirmed by qRT-PCR in Ctrl and *B40* OE MIN6 cells (n = 3; **C**) or Ctrl and *B40* KD MIN6 cells cultured under 20% or 5% O_2 for 24 hours (n = 3; **D**). (**E-F**) Western blot of BHLHE40 and MAFA expression in Ctrl and *B40* OE MIN6 cells (**E**) or Ctrl and *B40* KD MIN6 cells cultured under 20% or 5% O_2 for 24 hours (**F**). (**G**) qRT-PCR of MAFA target genes in Ctrl and *B40* KD MIN6 cells cultured under 20% or 5% O_2 for 24 hours (n = 3). (**H**) Glucose-stimulated insulin secretion in MIN6 cells infected with AAV-green fluorescent protein (GFP) (Ctrl) or AAV-*Mafa* and cultured under 20% or 5% O_2 for 24 hours (n = 4). (**I**) KCl-stimulated insulin secretion in MIN6 cells infected with AAV-GFP (Ctrl) and AAV-*Mafa* and cultured under 20% or 5% O_2 for 24 hours (n = 4). Data are mean ± SEM; *p < 0.05, *p < 0.01 and ***p < 0.001 by unpaired two-tailed Student's *t* test. β-actin was used as a loading control. Ctrl, control.

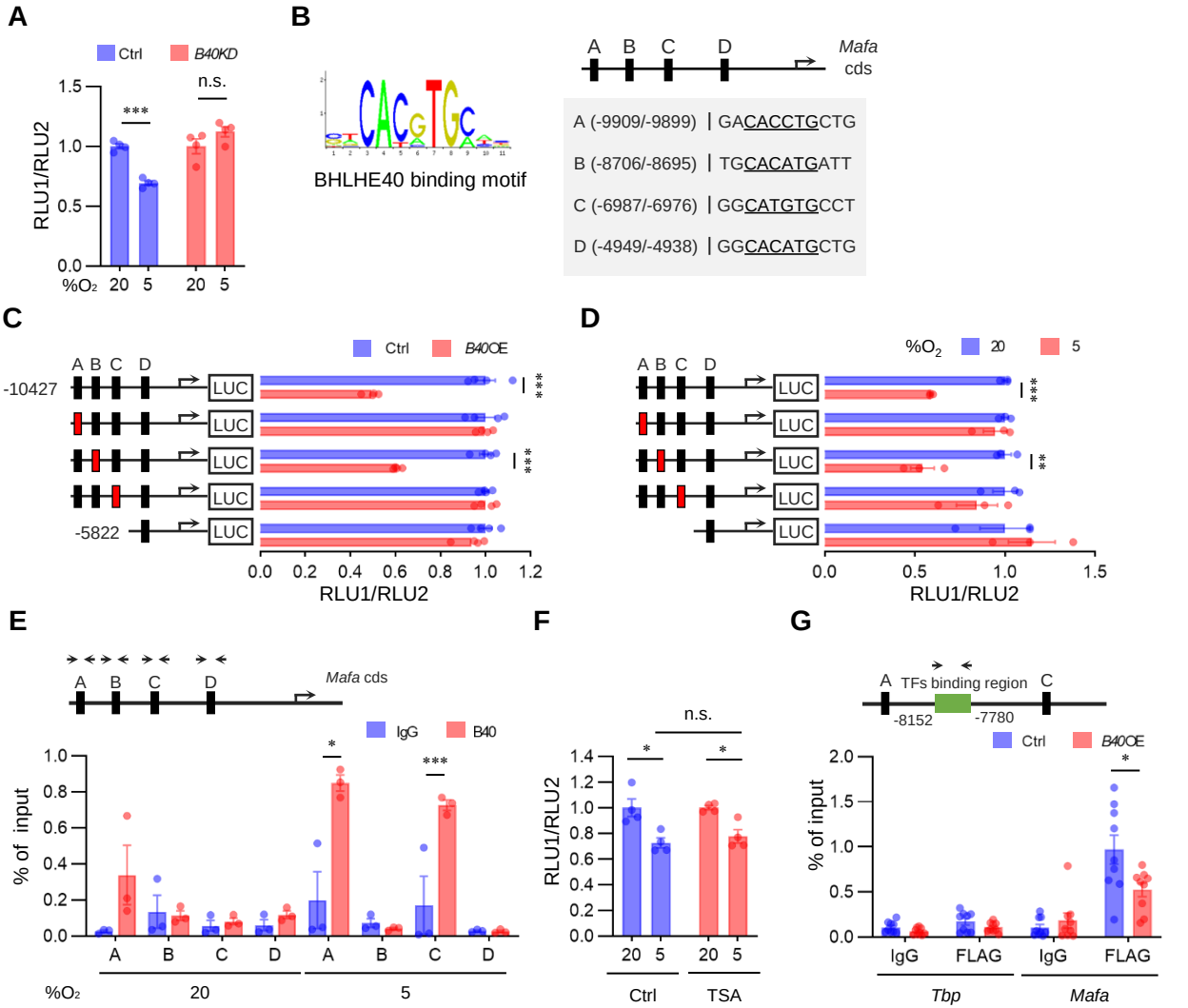
A
Ctrl
B40KD
n.s.
***
RLU1/RLU2
%O2 20 5 20 5
B
BHLHE40 binding motif
A B C D
Mafa cds
A (-9909/-9899) | GACACCTGCTG
B (-8706/-8695) | TGCACATGATT
C (-6987/-6976) | GGCATGTGCCT
D (-4949/-4938) | GGCACATGCTG
C
Ctrl
B40OE
-10427
-5822
LUC
RLU1/RLU2
D
%O2 20 5
RLU1/RLU2
E
Mafa cds
IgG
B40
% of input
%O2 20 5
F
n.s.
RLU1/RLU2
Ctrl TSA
G
TFs binding region
-8152
-7780
Ctrl
B40OE
% of input
IgG FLAG IgG FLAG
Tbp Mafa

Figure 5. BHLHE40 controls *Mafa* expression via two E-box sites in the enhancer region. (**A**) Reporter gene analysis with luciferase plasmid infused with mouse MAFA promoter/enhancer (-10427/+22 bp from transcription start site) in Ctrl and *B40* KD MIN6 cells cultured under 20% or 5% O_2 for 24 hours (n = 4). (**B**) BHLHE40-binding motif (upper left) and JASPAR results (lower left) are presented. JASPAR predicted four E-box sites for BHLHE40 binding on MAFA promoter/enhancer (relative score > 0.9, E-box sites are underlined). (**C**) Luciferase reporter assay was performed with MIN6 cells transfected with BHLHE40 expression plasmids, pRL-SV40 plasmid, and pGL3-Mafa plasmids (wildtype [black] and E-box mutated [red] sites; n = 4). (**D**) Luciferase reporter activity in MIN6 cells cultured under 20% or 5% O_2 for 24 hours (n = 3). (**E**) MIN6 cells were cultured in 20% or 5% O_2 for 24 hours, and then the proteins were immuno-precipitated by IgG or anti-BHLHE40 specific antibody, after which qRT-PCR was performed for the indicated regions (n = 3). (**F**) Luciferase reporter assay in MIN6 cells incubated with 0.1μM TSA or vehicle for 24 hours (n = 4). (**G**) Proteins sampled from Ctrl and *B40* OE MIN6 cells with FLAG-Pdx1 expression were immuno-precipitated by IgG or anti-FLAG antibody, after which qRT-PCR was performed for the indicated regions (n = 9). Data are mean ± SEM; *p < 0.05 **p < 0.01, and ***p < 0.001 by unpaired two-tailed Student's *t* test. Ctrl, control; n.s., not significant.

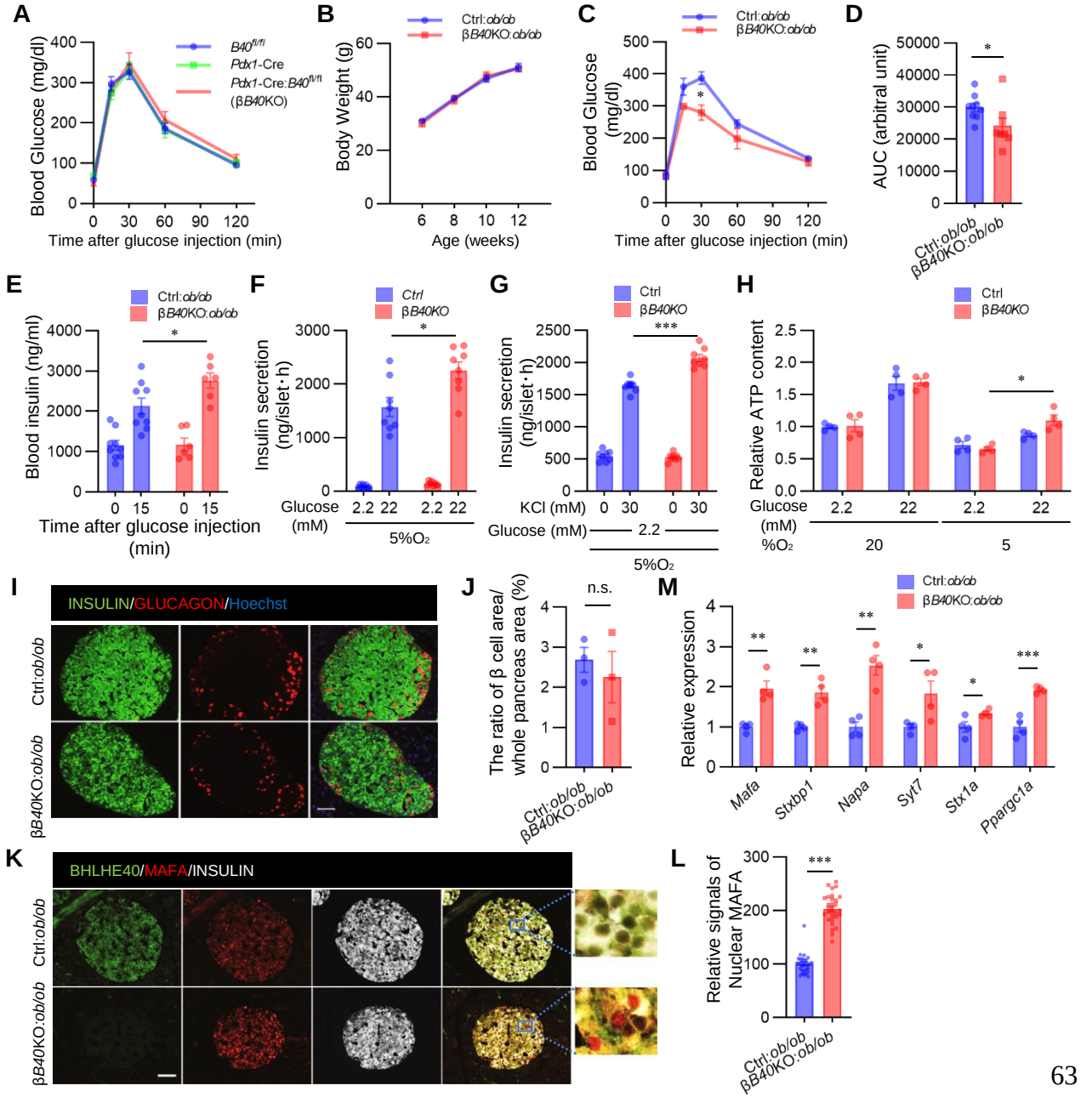
A
Blood Glucose (mg/dl)
Time after glucose injection (min)
B40fl/fl
Pdx1-Cre
Pdx1-Cre:B40fl/fl
(βB40KO)
B
Body Weight (g)
Age (weeks)
Ctrl:ob/ob
βB40KO:ob/ob
C
Blood Glucose (mg/dl)
Time after glucose injection (min)
D
AUC (arbitral unit)
E
Blood insulin (ng/ml)
Time after glucose injection (min)
F
Insulin secretion (ng/islet·h)
Glucose (mM)
5%O2
G
Insulin secretion (ng/islet·h)
KCl (mM)
Glucose (mM)
5%O2
H
Relative ATP content
Glucose (mM)
%O2
I
INSULIN/GLUCAGON/Hoechst
J
The ratio of β cell area/ whole pancreas area (%)
n.s.
M
Relative expression
Mafa
Stxbp1
Napa
Syt7
Stx1a
Ppargc1a
K
BHLHE40/MAFA/INSULIN
L
Relative signals of Nuclear MAFA

Figure 6. Deficiency of BHLHE40 improves hyperglycaemia in *ob/ob* mice. (**A**) Glucose tolerance test of *Pdx1*-Cre (*Cre*), *Bhlhe40*$^{fl/fl}$ (*B40*$^{fl/fl}$), and *Pdx1*-Cre:*Bhlhe40*$^{fl/fl}$ (*Cre:B40*$^{fl/fl}$) mice (n = 7, n = 12, and n = 9 respectively; 8-12 weeks old). (**B**) Body weight of *Bhlhe40*$^{fl/fl}$ (Ctrl):*ob/ob* and *Pdx1*-Cre:*Bhlhe40*$^{fl/fl}$ (βB40KO):*ob/ob* mice (n = 9 and n = 6, respectively). (**C** and **D**) Glucose tolerance test of Ctrl:*ob/ob* and βB40KO:*ob/ob* mice (n = 9 and n = 8, respectively; 6 weeks old) (**C**) and AUC (**D**). (**E**) Glucose-stimulated insulin secretion in Ctrl:*ob/ob* and βB40KO:*ob/ob* mice (n = 9 and n = 6, respectively; 8 weeks old). (**F**) Glucose-stimulated insulin secretion in isolated islets from Ctrl and βB40KO mice after culture under 5% O_2 for 24 hours (n = 8). (**G**) KCl-stimulated insulin secretion in isolated islets from Ctrl and βB40KO mice after incubation with 5% O_2 for 24 hours (n = 8). (**H**) ATP content in isolated islets of Ctrl and βB40KO mice after incubation with 20% or 5% O_2 for 24 hours (n = 4). (**I** and **J**) Representative images of pancreatic islets stained for insulin and glucagon in Ctrl:*ob/ob* and βB40KO:*ob/ob* mice (12 weeks old) (**I**). The ratios of total islet area to whole pancreas area (%) are shown (n = 3; **J**). (**K** and **L**) Representative images of pancreatic islets stained for insulin, MAFA, and BHLHE40 in Ctrl:*ob/ob* and βB40KO:*ob/ob* mice (12 weeks old) (**K**). Fluorescence intensities of nuclear and cytosolic MAFA in **K** were quantified (n = 30; **L**). (**M**) qRT-PCR of *Mafa* and its target genes in Ctrl:*ob/ob* and βB40KO:*ob/ob* mice (n = 4). Data are mean ± SEM; *p < 0.05 **p < 0.01, and ***p < 0.001 by unpaired two-tailed Student's *t* test. Scale bar, 10 μm. Ctrl, control; n.s., not significant.

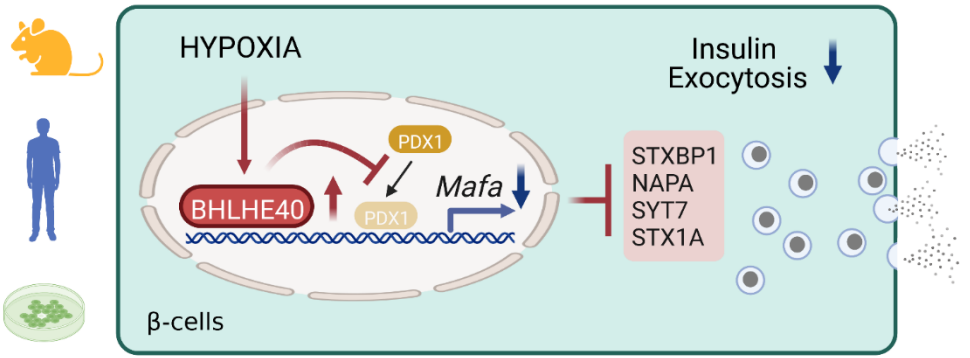

Figure 7. A proposed model for how hypoxia causes β-cells dysfunction.